



MiniSShot

Launch Report

Rev. 2010/08/15

Introduction

This report is a documentation of the first launch of the *MiniSShot* rocket vehicle which took place on April 25, 2010 at the FAR test site in the Mojave Desert. The launch was in support of the goal of the *MiniSShot* Project, namely to develop, launch and recover a 1/3 scale version of the planned *ExSShot* space rocket. The altitude goal for this flight was approximately 40k feet (12.2 km) as detailed in References 1 & 2. Due to a catastrophic motor malfunction at the beginning of the second burn, the actual apogee attained was 12k feet (3.7 km). All major parts of the vehicle were recovered following breakup that was initiated by the malfunction. Notably, the Payload Capsule was recovered fully intact, having descended under safety of its main parachute.

General Description

The *MiniSShot* rocket consists of two sections: Booster and Payload Capsule. These two sections are designed to separate at apogee and descend separately. The Booster consists of rocket motor and Aft Avionics Bay. The Payload Capsule consists of Nosecone and Recovery Bay. Most of the avionics are housed in the nosecone and forward portion of the Recovery Bay. The parachutes are housed in the aft portion of the Recovery Bay. Total length of the 3.5" (89 mm) rocket, from nozzle exit to nosecone tip is 11.5 ft (3.49 metres). Lightweight composite materials are used extensively, including motor casings, airframe, nosecone and fins. Liftoff mass was 44.5 lbs (20.2 kg), propellant mass was 24.0 lbs (10.9 kg), providing for a vehicle mass fraction of 0.54. Estimated masses used for design and analysis are provided in Reference 3. Reference 4 describes the vehicle assembly and launch readiness procedure.

Booster

The Booster is an N-class solid propellant rocket motor which has a novel dual-phase operation. Two propellant charges are housed in separate stacked chambers isolated by a "delay plug" integrated into the Mid-bulkhead. The propellant charge in the aft chamber fires first. After a ten second "coast delay", during which time the "delay plug" burns away, the charge in the second chamber fires. The grain configuration is BATES with 6 grain segments in each chamber. The motor was first successfully test fired as *ProtoSShot-M Mark III* on July 25th, 2009 at the FAR static test facility in the Mojave Desert (Ref.5). Table 1 provides basic details on the motor and performance. Reference 6 details the procedure used for rocket motor assembly and propellant loading.

| | |
|-----------------------|---|
| Propellant type | KNSB |
| Propellant mass | 24.0 lb (10.9 kg) total for both chambers |
| Design Impulse | 7000 N-sec. total |
| Delay between firings | 11 sec. nominal |
| Throat diameter | 0.792 in (20.1 mm) |
| Expansion ratio | 10:1 |
| Igniter | Main charge: 10 g. CuO/Al thermite (each chamber) Initiator: <i>J-Tek</i> electric match |

Table 1 – Motor basic details

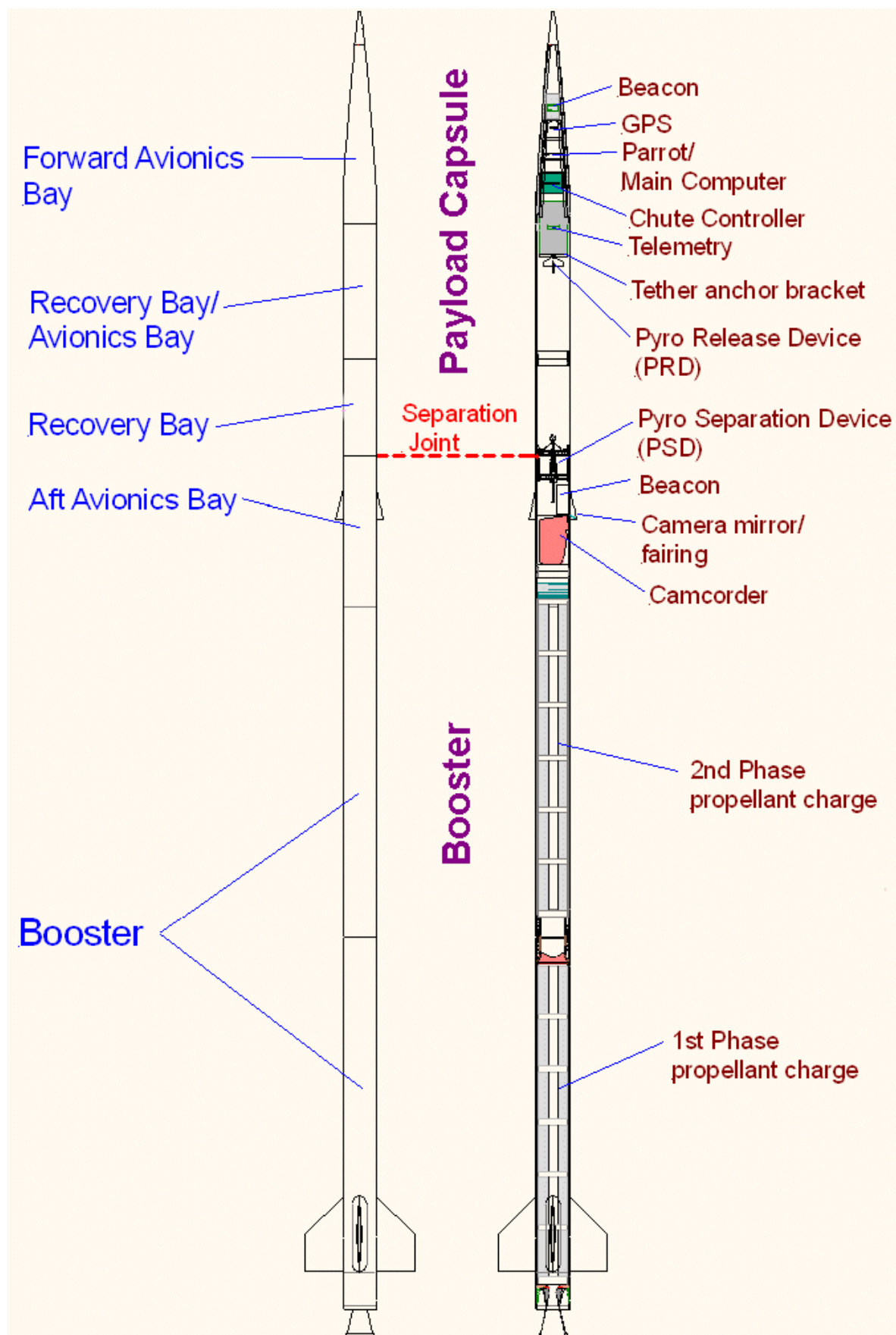


Figure 1 – Overview of the vehicle

Propellant

Propellant was conventional KNSB, consisting of 65% potassium nitrate and 35% sorbitol. Both constituents, “as obtained”, were weighed out, placed in a large ball mill, and blended for xx hours. The entire dry-mix batch, enough for 12 grain segments, was prepared as a single batch. The batch of dry-mix was then bagged into 12 individual batches, each enough for one segment plus wastage. Casting was performed using the standard process and the same apparatus as for the *ProtoSShot-M* motor firings. The casting tubes were custom-fabricated of a high performance ablator (SSA-3, aft tubes; SSA-2, forward tubes), custom developed for this application.

To ensure grains of acceptable quality were produced, a density check, visual inspection and coin tap test were performed. Density check was to ensure minimal air intrusion and to ensure the grain was void-free, visual inspection to ensure no cracks or defects along the core or end surfaces, and the tap test to confirm positive bonding between the propellant and casting tube.

Primarily as a result of thermal shrinkage, the amount of propellant after casting was less than desired. A decision was made to “top off” each of the grain segments by adding a 5 mm layer of additional propellant. Three measures were taken to validate the “topping off” technique, since this had not been done before. A calculation was done to verify that chamber pressure would be within acceptable limit if disbonding of all the propellant layers occurred. Another was to check the bond of the topped off layer by attempting to pry off the layer. This test was done on each of the twelve grains. The result was negative, with the bond holding fast in each case. As well, two sample “topped off” grains were prepared for a test motor that was successfully fired (albeit no pressure or thrust measurements were recorded due to instrumentation glitch).

Ignition primer was painted on all grain segment ends, as was done for all *ProtoSShot-M* static firings. It was decided to also fully paint all the cores. Previously, cores were painted only to within one inch (2.5 cm) of each end. The justification for this modification was the desirability of faster motor startup and resulting improved motor performance.

Appendix A provides the details of the twelve grain segments prepared. The grains were all cast in January 2010 and topped off in February.

Recovery System

Dual deployment was employed for the Payload Capsule, single deployment for the Booster. At apogee, following separation of the Booster and Payload Capsule, the Booster chute and the Payload Capsule drogue are deployed. The main chute for the Payload Capsule is deployed at an altitude of 800 metres AGL. Parachute details are provided in Table 1.

| Recovery Parachutes | | | |
|------------------------|-------------|---------------------|--------|
| | Type | Diameter (inflated) | Colour |
| Booster | Parasheet ? | 18” (46 cm) ? | orange |
| Payload Capsule drogue | Parasheet ? | 12” (31 cm) ? | TBA |
| Payload Capsule main | Parasheet ? | 30” (76 cm) ? | white |

Table 2 – Recovery parachute details

Note: “?” signifies tentative data, to be confirmed

Prior to separation at apogee, the Pyro Separation Device (PSD) serves as a structural joint, connecting the Booster to the Payload Capsule. At apogee, an electrical signal from the redundant recovery system avionics (Chute Controller & Parrot) fires the (PSD), which forcibly separates the two sections. As a result, the two apogee chutes are pulled out and immediately deploy. The main chute is later withdrawn from the Recovery Bay when an electrical signal from the Chute Controller fires the Pyro Release Device (PRD). Drag force developed by the drogue serves to extract the main chute.

The procedure used for assembling the PSD is provided in Reference 7.

Design touchdown velocity for the Booster is 87 fps (26.5 m/s), terminal velocity for the Payload Capsule under drogue is 82 fps (25 m/s) and touchdown velocity for the Payload Capsule under main is 32 fps (9.8 m/s).

Avionics

Table 3 lists the various avionics packages and Reference 8 illustrates, in the form of a Block Diagram, the interfacing of the various components. References 9 through 15 provide description of the various avionics and the checklist procedures used in preparation for launch.

| Forward Avionics Bay | Model/SN | Manufactured by | Power Supply |
|----------------------------------|---|-----------------------------------|---|
| Chute Controller (CC) | SN 03 | Hans Olaf Toft | <i>Impulse Power</i> 7.4V 480mAh LiPo (and 9V BEM) |
| Main Computer (MC) | SN 008 | Hans Olaf Toft | <i>TANIC TAPS</i> 11.1V 1550mah LiPo (Battery A) |
| Thermal Board & Nosecone sensors | - | Andre Alexandre Barbosa Stavrakas | <i>TANIC TAPS</i> 11.1V 1550mah LiPo (Battery A) |
| Parrot Altimeter | <i>Parrot V2.0</i> | <i>Featherweight</i> | Board: built-in 4.2V LiPo |
| Recovery Beacon | <i>BeeLine</i> | <i>Big Red Bee, LLC</i> | 3.7V LiPo |
| Beacon amplifier | <i>AMP-900 TX</i> | <i>RF Links</i> | <i>TANIC TAPS</i> 11.1V 1550mah LiPo (Battery B and 9V BEM) |
| GPS module/antenna | - | <i>Holux</i> | <i>TANIC TAPS</i> 11.1V 1550mah LiPo (Battery A) |
| Telemetry transmitter | <i>TinyTrak</i> | <i>Byonics</i> | <i>TANIC TAPS</i> 11.1V 1550mah LiPo (Battery A) |
| ATV transmitter | <i>ATV12-915 1.5W 3 CH 900 MHz ATV XMTR</i> | <i>North Country Radio</i> | <i>TANIC TAPS</i> 11.1V 1550mah LiPo (Battery A) |
| Patch antenna | - | Peter Kocalka | - |

| Aft Avionics Bay | Model/SN | Manufactured by | Power Supply |
|-------------------------|-----------------|------------------------|---------------------|
|-------------------------|-----------------|------------------------|---------------------|

| | | | |
|-------------------|--|-------------------------|---|
| Recovery Beacon | <i>BeeLine</i> | <i>Big Red Bee, LLC</i> | Factory attached LiPo |
| Beacon amplifier | - | Chris King | <i>Impulse Power</i> 11.1V LiPo (and 9V BEM) |
| HD mini-camcorder | <i>moviePix HD MP5A4</i> 8 megapixel;1280x720 16:9 ratio@ 30 fps | <i>Kobian</i> | 3.7V 1200 mAh LiPo |

Table 3 – Avionics details

The Main Computer logs the position data from the *Holux* GPS at the 1 hz. rate at which data become available. The Chute Controller records data at a 100 ms rate, beginning at liftoff (based on a launch-detect algorithm) and the Parrot at a 5 ms rate, beginning just prior to launch. The CC not only records the barometric data it, but also performs a real-time conversion into (raw) altitude that is fed into a Kalman filter that provides an improved altitude estimate (AGL). Both the CC and Parrot sense barometric pressure, which is converted to altitude using Standard Atmosphere or radiosonde data. To ensure accurate barometric sensing, the nosecone attachment joint is sealed with an o-ring, and the Payload Capsule carefully sealed with the exception of 4 static ports (1.5 mm Ø) located just forward of the separation joint.

The mini-camcorder is configured to shoot in an aft-facing direction, by use of an externally mounted first-surface mirror, tilted at approximately 45 degrees. An aerodynamic fairing houses the mirror. An identical dummy fairing is mounted on the opposite side of the airframe to provide balanced drag. Reference 17 describes the procedures for setting up the camcorder for flight. The camcorder was fitted with a 4 Gb SD card which allows for 2 hours of HD recording. The battery was ground tested and demonstrated to provide over 2 hours of recording life on a full charge.

The nosecone was fitted with four RTD temperature sensors embedded in the outer skin. The sensors were connected to a conditioning circuit board which was directly mounted on and interfaced to the MC for data recording. Although no significant thermal heating of the nosecone skin is expected for this flight, the main purpose of including this payload is to test out the concept which will be important for future projects which will achieve much higher velocities.

Some ‘last minute’ changes were made to the avionics which accounts for differences between the configuration shown in the Block Diagram (Ref.8) and actual configuration. The *Byonics* GPS unit originally slated was replaced by the *Holux* unit as indicated in Table 3. Ground testing indicated that the original unit was not functioning properly, damage being attributed to handling and attempting to fit the unit into very limited space in the avionics compartment. Another change was to the Payload Capsule beacon amplifier. Due to similar space limitation, a commercially obtained unit, as indicated in Table 3, was used instead of the custom manufactured unit. The vibration sensor and DTMF backup system were not included in this flight, due to delivery problems from Brazil where these components were being fabricated or integrated.

Launch Platform

The *MiniSShot* vehicle was launched from an adjustable, four-guide-pole tower on-loan from Dok Hansen. As a benefit of using a tower platform, no external lugs or other provisions were fitted to the vehicle. The launch angle was set to zero degrees from vertical.

Tracking and Recovery

Two teams collaborated to track and recover the *MiniSShot* vehicle. *Stratofox* team supplied six trackers and *SAR* supplied six trackers. *Stratofox* is a team of Amateur Radio operators who participate in tracking and recovery operations for amateur, entrepreneurial and research rocketry and high-altitude balloon flights. *SAR* is a local organization of search and rescue volunteers.

Launch

Weather conditions - Weather conditions were ideal, with clear skies and light wind. The ambient temperature was around 75° F (24° C). Winds aloft forecast, issued the day prior to launch, is provided in Table 4.

| 25-APR | | | |
|--------|-----|-----|-----|
| ALT FT | DIR | SPD | TMP |
| 5000 | 070 | 11 | 14 |
| 10000 | 201 | 2 | 4 |
| 15000 | 317 | 9 | -6 |
| 20000 | 332 | 10 | -18 |
| 25000 | 347 | 15 | -30 |
| 30000 | 351 | 11 | -43 |
| 35000 | 307 | 18 | -54 |
| 40000 | 288 | 36 | -60 |
| 45000 | 280 | 40 | -60 |
| 50000 | 278 | 40 | -62 |

ALTITUDES ARE MEAN SEA LEVEL.
WIND DIRECTION IS TRUE DEGREES, SPEED IS IN KNOTS.
TEMPERATURE IS IN DEGREES CELSIUS.

Table 4- Winds aloft forecast for launch day

Pre-launch setup and checkout – Assembly of various components such as the motor was done the day before launch. The tracking teams practiced and performed simulated tracking and recovery operations, which was enhanced by the launch of a small conventional rocket. Motor igniters were prepared and ground tested. It was decided, based on these igniter tests, that a single *Pyrodex* pellet be included in the second-phase igniter to provide greater reliability of thermite initiation. On the morning of the launch, final vehicle preparations and setup of the avionics was performed. The Booster section was installed in the launch tower, the tracking beacon powered and the camcorder recording began. The Payload Capsule was then mated to the Booster, following activation and arming of the recovery devices. The final preparations for launch took longer than expected pushing back liftoff time from the planned 8AM to 10AM. The tracking teams, meanwhile, assumed their positions, prepared their equipment, and awaited notification of countdown by radio. There were some issues with reception of the telemetry signal. Being a non-critical system, the launch was given a go-ahead. Just prior to countdown, the second phase igniter safety shunt was pulled using a long string. Although contrary to instructions in Ref.4, it was felt that personnel safety was enhanced without significant risk of perturbing the on-board electronics using this ad hoc method.

Launch - The *MiniSShot* rocket was launched at 10:03 AM PDT (17:03 UTC) April 25, 2010. Ignition occurred promptly at “zero” and liftoff was brisk. The rocket rapidly accelerated skyward and ascended in a straight vertical trajectory. Burnout of the first phase occurred as expected approximately four seconds after ignition. The rocket coasted upward, continued on a stable, nearly vertical ascent. A light smoke trail was visible during the coast, as expected from the burning delay plug and pyrolyzing casting tube ablator. Ignition of the second phase was seen to occur approximately 11 seconds later, as indicated by the sudden appearance of a smoke cloud. Very shortly after, the rocket began to veer from vertical ascent and began a spiral course. About a second later, after performing two spiral loops, the trajectory suddenly straightened. A loud “boom” was then heard. Although not apparent at the time, the sound (delayed by the distance) was from the rupture of the aft motor casing. The ground video later showed that rupture was accompanied by several pieces of smouldering debris being scattered, later identified as spent casting tubes and the aft half of the fractured booster. The second phase burn continued for ten seconds, propelling the vehicle along a stable but erratic path. The burn time was much greater than nominal as a result of nozzle not being present. Observers spotted an unidentified section of the vehicle descending, suspended under a white parachute, and visually followed it to the ground. It touched down after about seven minutes. The section turned out to be the Payload Capsule, which was found inverted with the nosecone tip stuck in the soft ground. There was no visible damage. The Booster was later recovered in two separate pieces. The forward portion of the Booster impacted the ground with significant force, contacting at the forward end, resulting in damage to the casing, PSD and camcorder support structure. The aft (finned) portion of the booster descended more rapidly. An observer reported that it had descended making a ‘wavering whistling’ sound, followed by a ‘thud’ and the appearance of a dust cloud at the impact site. The shredded Booster chute was also recovered and found nearby the Payload Capsule.

Post-recovery inspection and analysis of recovered components

The Payload Capsule, which descended by main parachute, was in good overall condition. There was some minor damage to the avionics support structure. However, all the electronic components were undamaged and flight data from the Chute Controller, Main Computer, and Parrot were successfully downloaded for post-flight analysis.

Overload due to high speed deployment of the drogue chute at the moment of vehicle breakup had snapped the tether connecting it to the main chute (it was designed such that the drogue tether would break away, in case of overload, before the main chute tether). The drogue chute was not recovered. The main chute did not suffer any damage.

The PRD was found to have fired and operated properly.

The PSD tether anchor bolt was still attached to the booster chute tether, it had snapped off the PSD where the threads began. Three of the pin-retaining holes in the PSD coupler ring exhibited shear tear-out with the fourth intact (photo 26). The tear-out is indicative of a high bending load experienced by the vehicle, likely during the spiraling motion following the anomaly. The spiraling may well have been a result of the booster chute causing asymmetric drag during the second phase burn, which continued until the tether snapped. The PSD body was damaged from ground impact, as

was the fiberglass dome plunger (Photo 24). The PSD igniter bridgewires were intact indicating it was not triggered.

The camcorder, located in the Aft Avionics Compartment was superficially damaged, however, rendered inoperable by the impact, and would not power-up. However, the SD card was intact and a 2 Gb file was downloaded. The file was corrupted but was later repaired by *AeroQuartet* video repair service and provided excellent footage of the ascent including the anomaly. Recording ceased as a result of the impact event with the ground. The Booster beacon sustained some superficial damage.

None of the casting tubes from the aft motor chamber were recovered. After an arduous extraction from the chamber, the forward casting tubes were found to be in similar condition to that seen after the *ProtoSShot III* static firing, with a slightly greater degree of thermal degradation. Photo x illustrates the tubes after cleaning and sectioning.

The Booster was found to have fractured approximately in the middle of the aft motor casing. All four fins were still attached to the aft portion, which was in good condition with the exception of the fracture (Photo 17). The inside surfaces of the casing did not display any sign of abnormal heating. The forward half of the aft motor casing remained attached to the Mid-bulkhead, and suffered severe heat damage due to the flow of the exhaust of the second phase combined with loss of the casting tubes which normally serve as a key part of the thermal protection system.

The Forward motor casing was in good overall condition with the exception of localized damage to the six holes which attach the coupler for the Aft Avionics housing (Photo 19). This damage appears to have occurred as a result of forces associated with ground impact. The interior walls of the casing experienced some heat related damage, although none greater than expected.

The Nozzle, Mid-bulkhead and Forward Bulkhead escaped unscathed. The ablative liners on the Nozzle and Mid-bulkhead exhibited normal erosion and did an effective job of providing thermal protection. The cork liner protecting the Forward Bulkhead also was effective.

Both the Payload Capsule radio beacon and the Booster beacon functioned as intended and the trackers successfully locked-in on signals which aided recovery. Ref. 18 is a debriefing document that summarizes tracking and recovery efforts.

Avionics Flight Data

The Main Computer (MC), Chute Controller (CC) and Parrot altimeter (?) each recorded a full data-set of the entire flight.

A plot of altitude versus time, based on CC data, is shown in Figure 2. Figure 3 shows the Parrot data in graphical form.

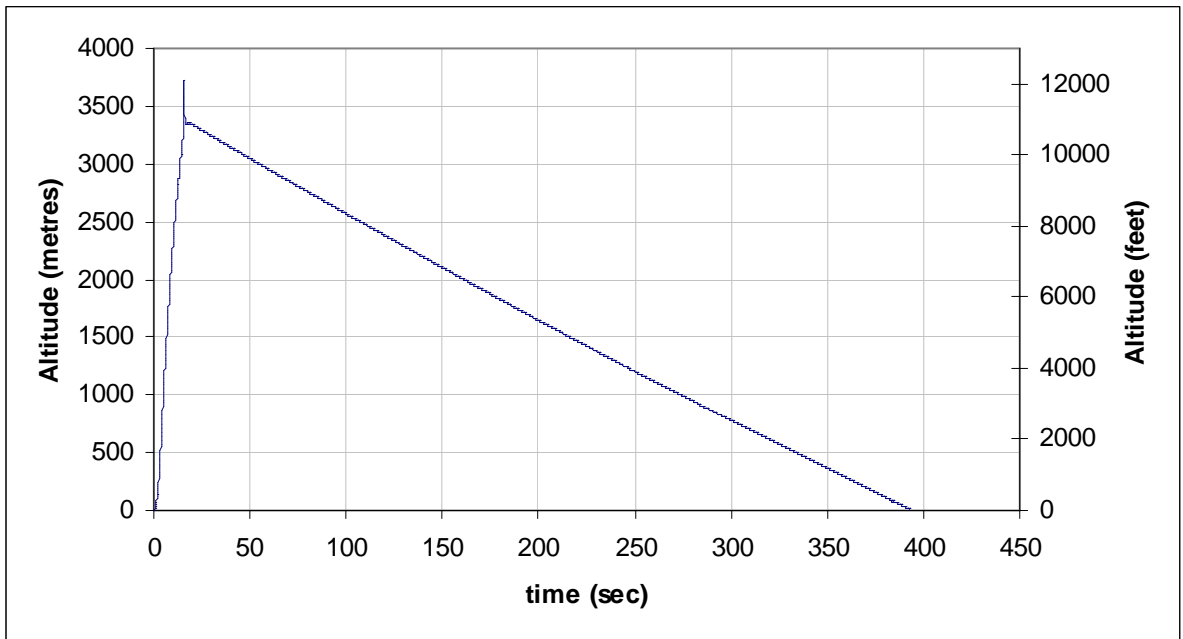


Figure 2 – Plot of CC altitude (AGL) versus time over entire flight

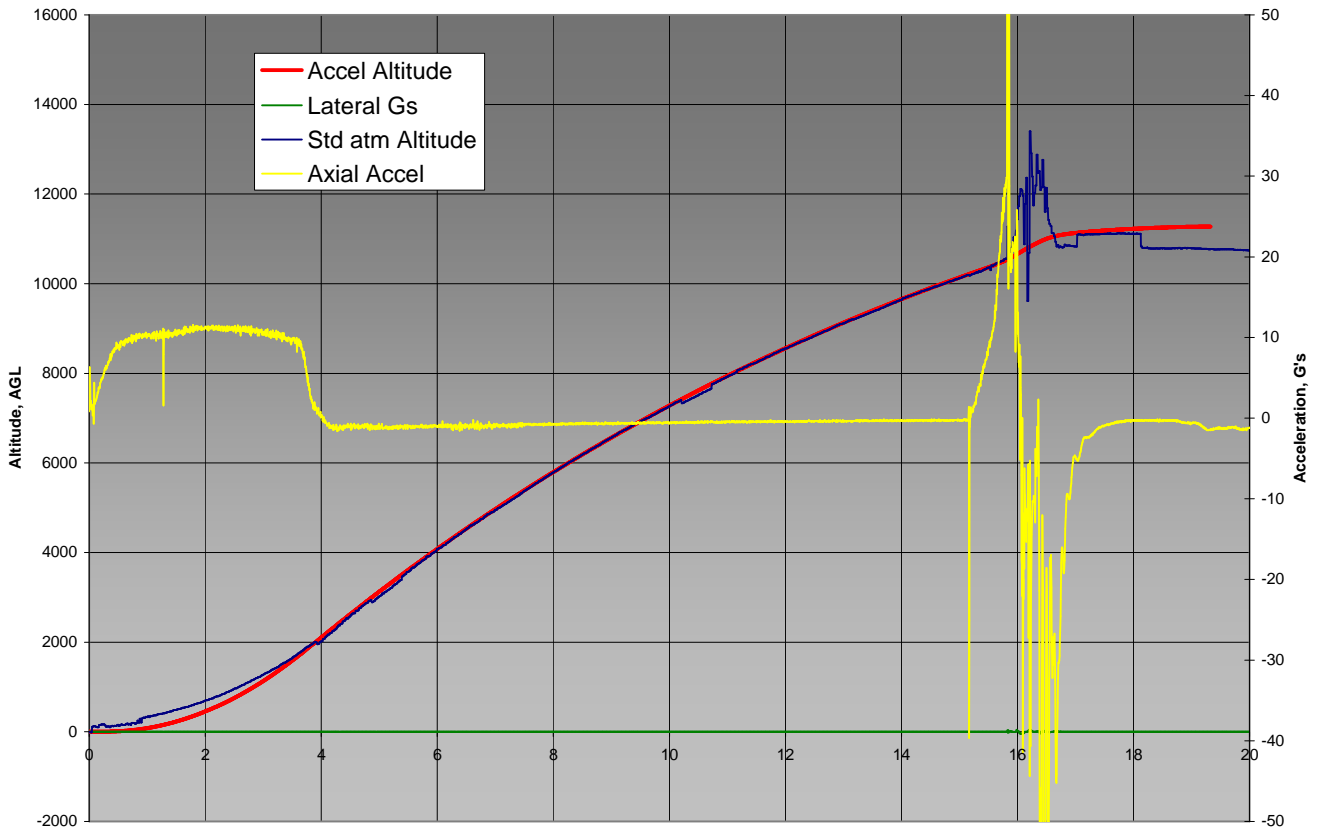


Figure 3 – Plot of Parrot flight data for the first 20 seconds

For supplemental CC calibration, data is available in the form of radiosonde data

(Vandenberg AFB being the most relevant radiosonde data available for the launch location & date). It is imported into the flight recordings by locating the matching barometric readings (in some cases the closest matching reading) and inserting the corresponding radiosonde altitude. The ground level altitude has been subtracted to get AGL readings. The results are shown in Figure 4.

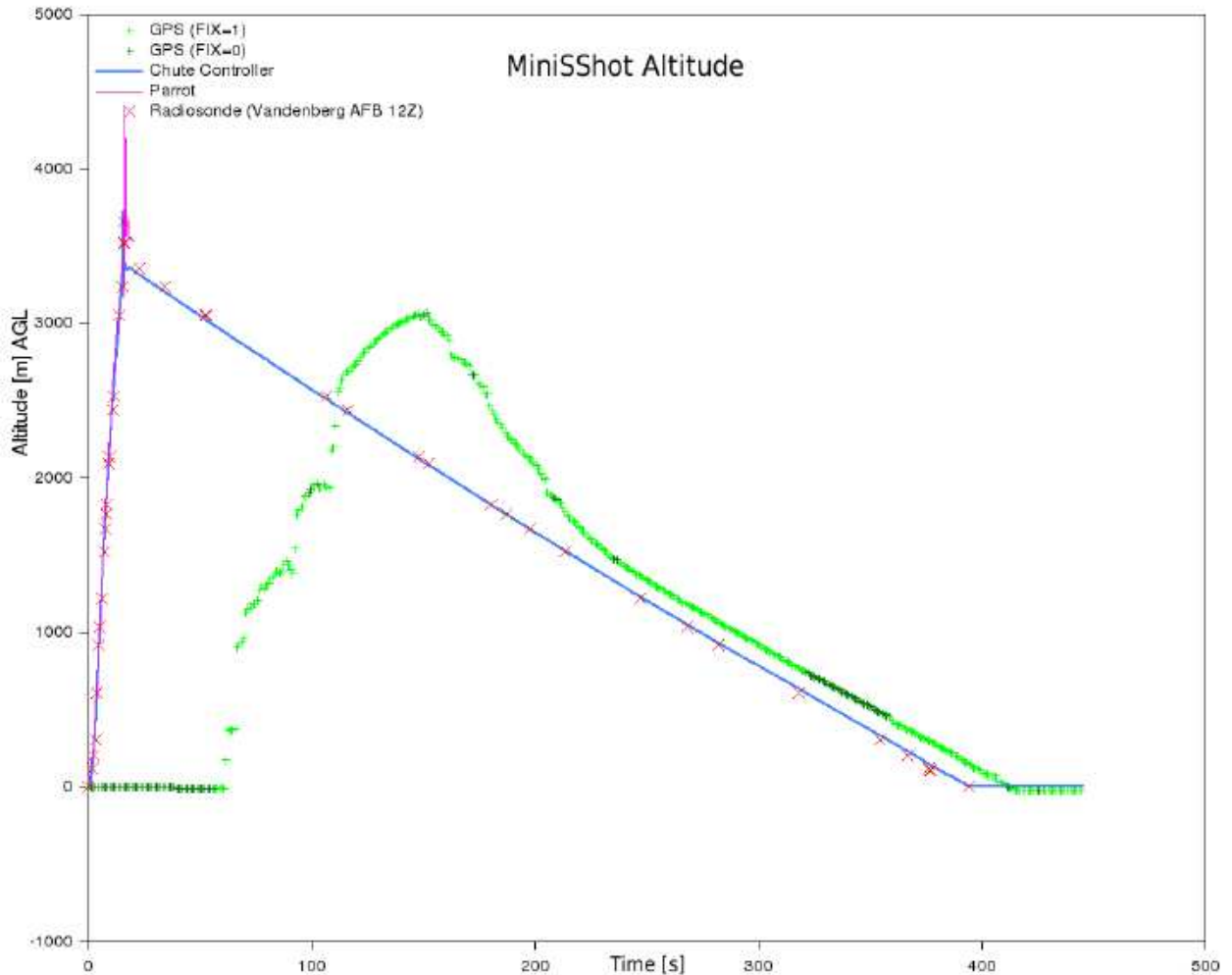


Figure 4 – Plot of GPS altitude with CC and Parrot altitude shown for comparison

The barometric altitudes match fairly well with each other and with the radiosonde data. The Parrot is being slightly more optimistic, estimating the altitude of the anomaly at 3475m while the CC estimates 3226m. The GPS data was rather peculiar. The GPS apparently loses lock at liftoff and regains lock after 56 seconds. At that time, the Payload Capsule is descending under chute, but the GPS signals a steep altitude increase, almost as if the rocket was ascending during powered flight. This “ascent” continues until the GPS signals an altitude of 3067m, roughly equivalent to that of the barometric altimeters. Then it signals descent at a faster rate than that of the barometric altimeters. Approximately halfway through the descent, the GPS descent rate converges and nicely matches that of the barometric sensors, however, retaining the time lag. It has been speculated that the GPS filters its position through a low pass filter, and that the apparent ascent is merely the step response of the internal filter, and that the apogee is simply a filter overshoot, coincidentally matching the barometric apogee. Another speculation is that the GPS stores position data internally but only releases it after regaining lock, compressing its timescale in order to catch up with reality.

The vehicle acceleration curve over the first 5 seconds is shown in Figure 5, followed by Figure 6 which details acceleration during the first 18 seconds. The MC and Parrot data are seen to be in close agreement. The MC data was “calibrated” by matching to the Parrot data, which is factory calibrated.

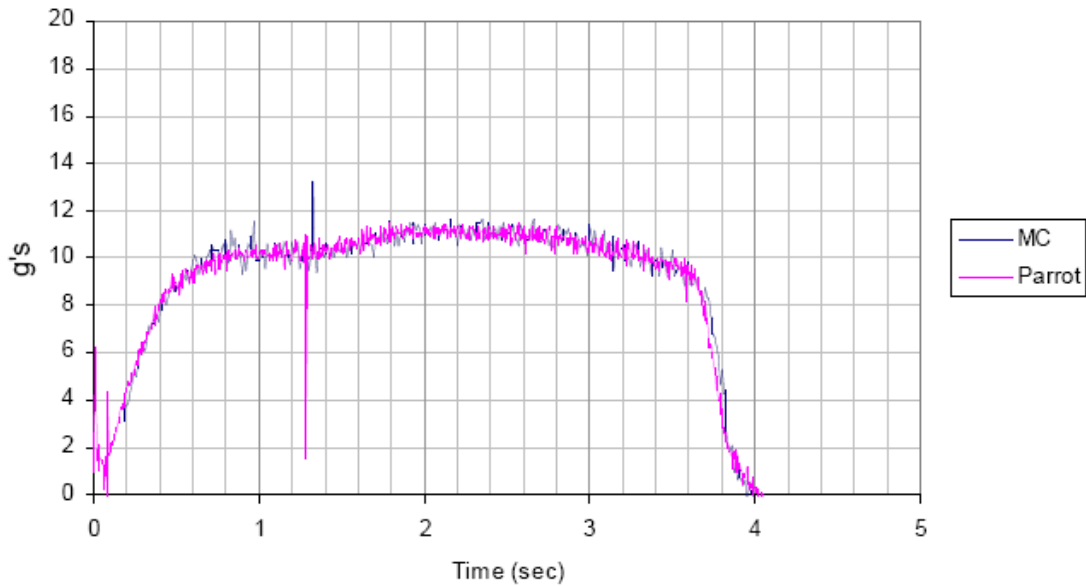


Figure 5 – Plots of acceleration during 1st burn

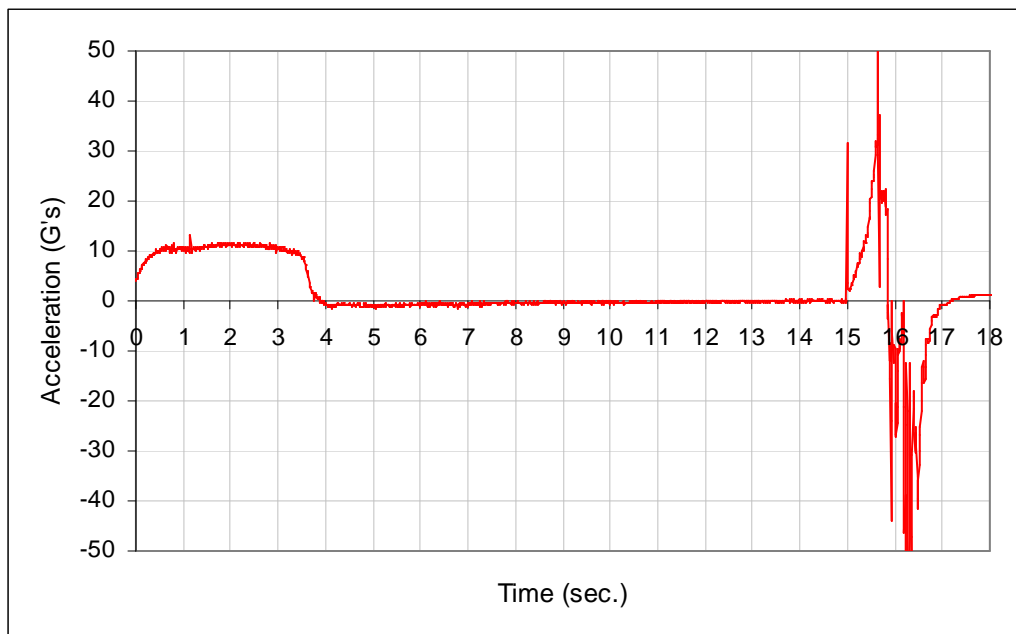


Figure 6 – Plots of MC acceleration data over the first 18 seconds of flight.

Figure 7 is a plot of vehicle acceleration during the 2nd phase burn and subsequent motor casing rupture. Two igniter events are shown. The first igniter event is “power on” to the booster igniter and the second event is loss of continuity of both the booster igniter and the CC pyro igniter. This

implies the event coincides with physical breaking of the igniter wires and thus separation of the Payload Capsule from the Booster.

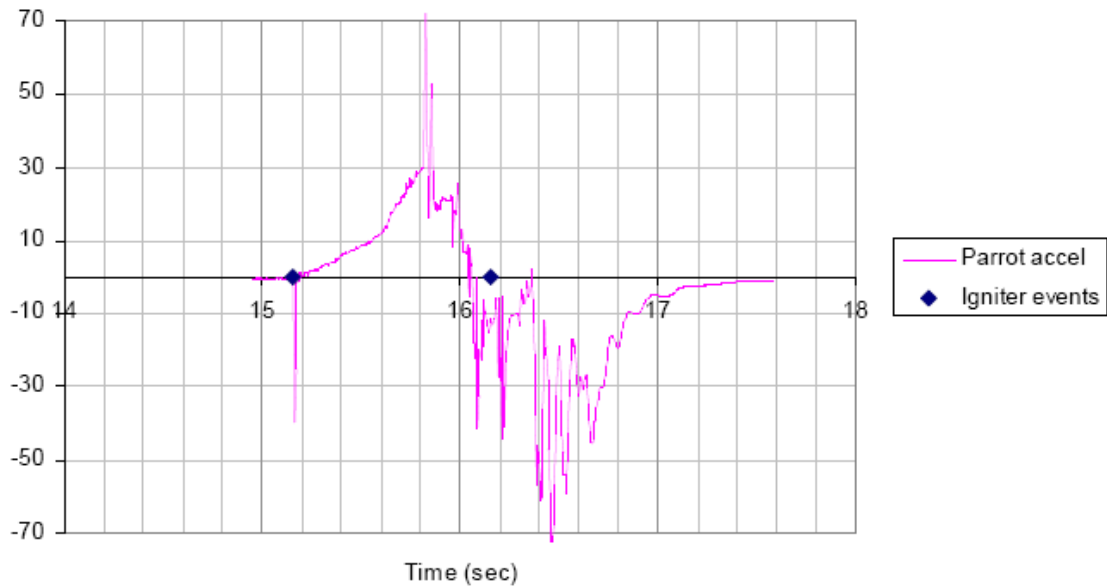


Figure 7 – Acceleration and motor igniter events for 2nd phase burn

Figure 8 is a plot of chamber pressure during the 2nd burn (note there was no provision for chamber pressure readings to be sensed during the 1st burn). In Figure 7 it can be seen that the pressure readings after separation are invalid as a result of severed electrical leads, which coincided (within a fraction of a second) with the second igniter event shown (loss of drogue pyro continuity). The pressure reading is clipped at 1130 psig, at which point the 1000 psi capacity transducer saturated.

MC chamber pressure and igniter events

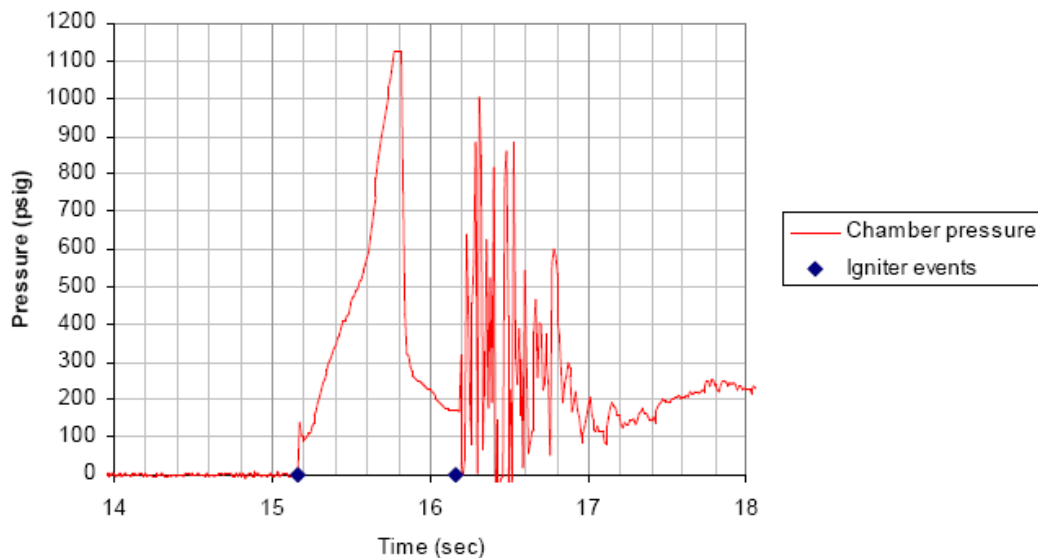


Figure 8 – Plot of chamber pressure sensor data

Figures 9 through 13 are plots of MC acceleration data..

Figure 9 is a plot illustrating the MC lateral accelerations data for the first 15 seconds of flight (from liftoff to just after occurrence of anomaly). Figure 10 focuses on the lateral accelerations during the first burn, and Figure 11 over the duration leading up to and immediately following ignition of the 2nd burn.

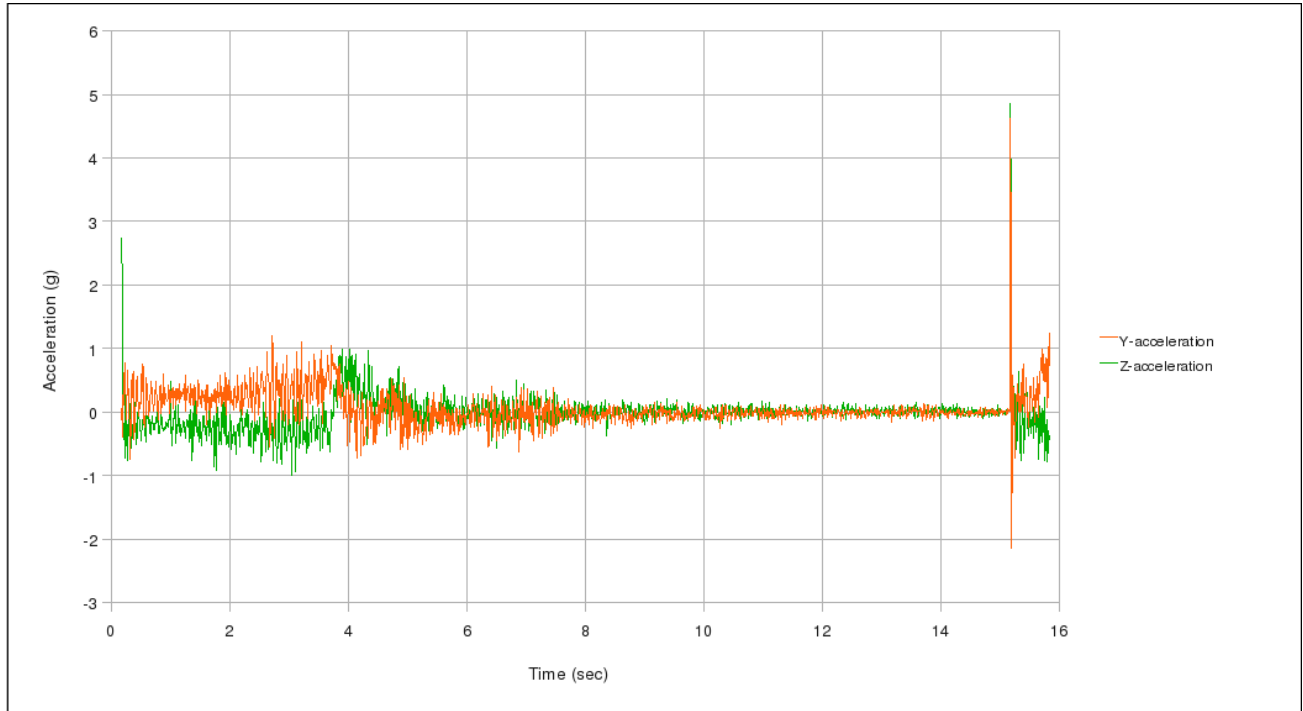


Figure 9 – Plot of lateral accelerations from liftoff until anomaly.

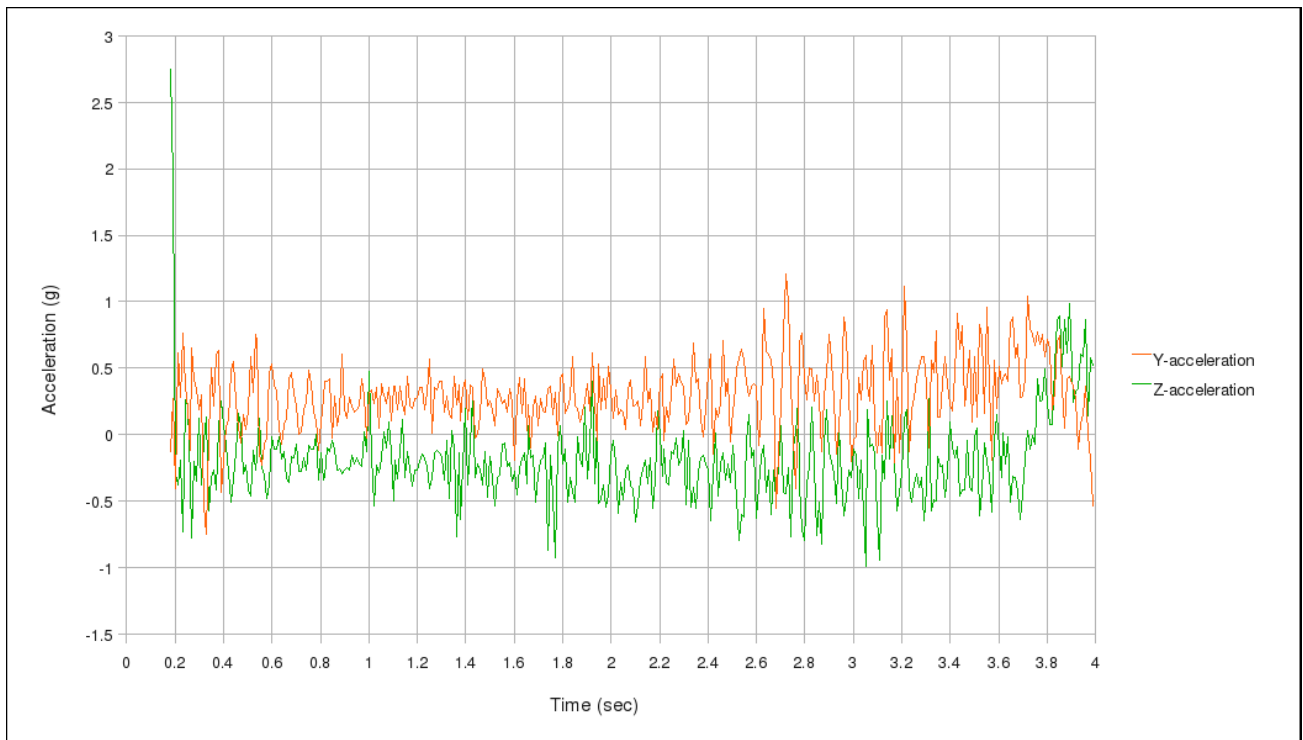
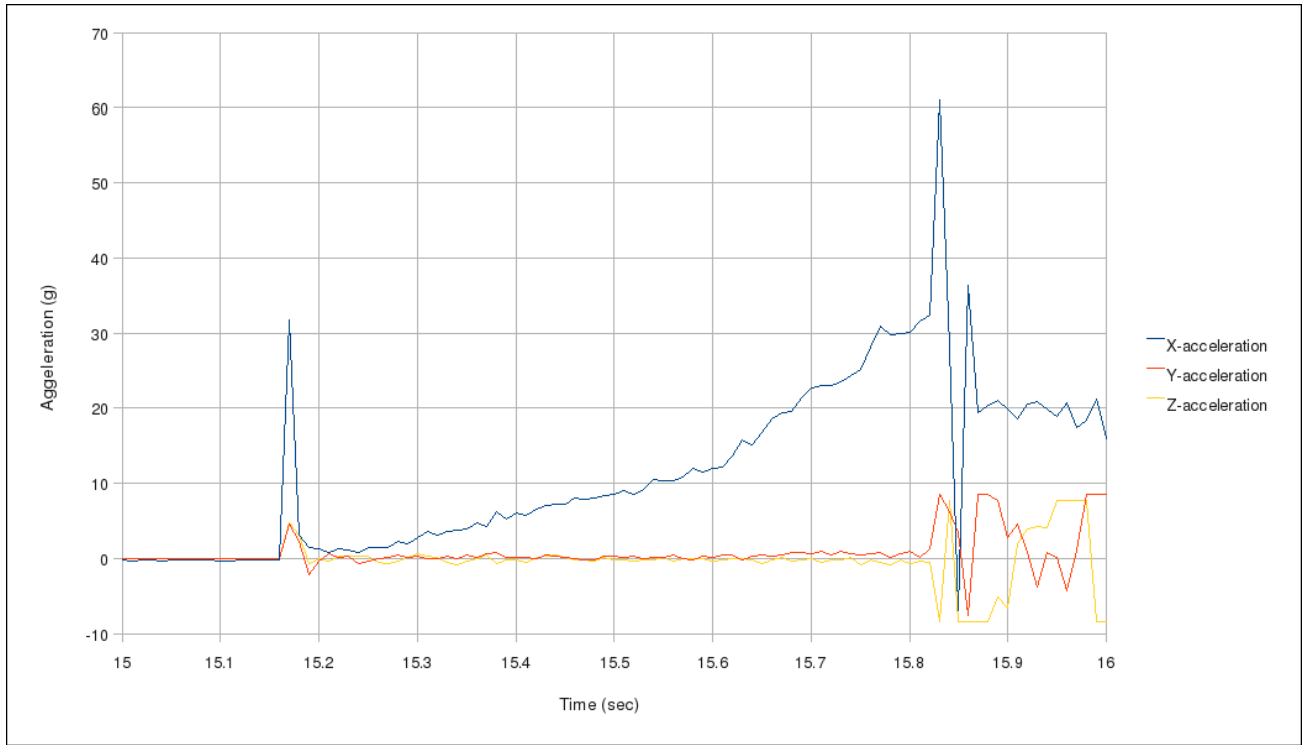


Figure 10 – Plot of lateral accelerations over duration of 1st burn



.Figure 11 – Plot of acceleration along 3 axes during 2nd burn

The angular accelerations of the vehicle are plotted in Figures 12 & 13, with x-omega representing “roll” and y-z accelerations representing “pitch” about the two perpendicular axes.

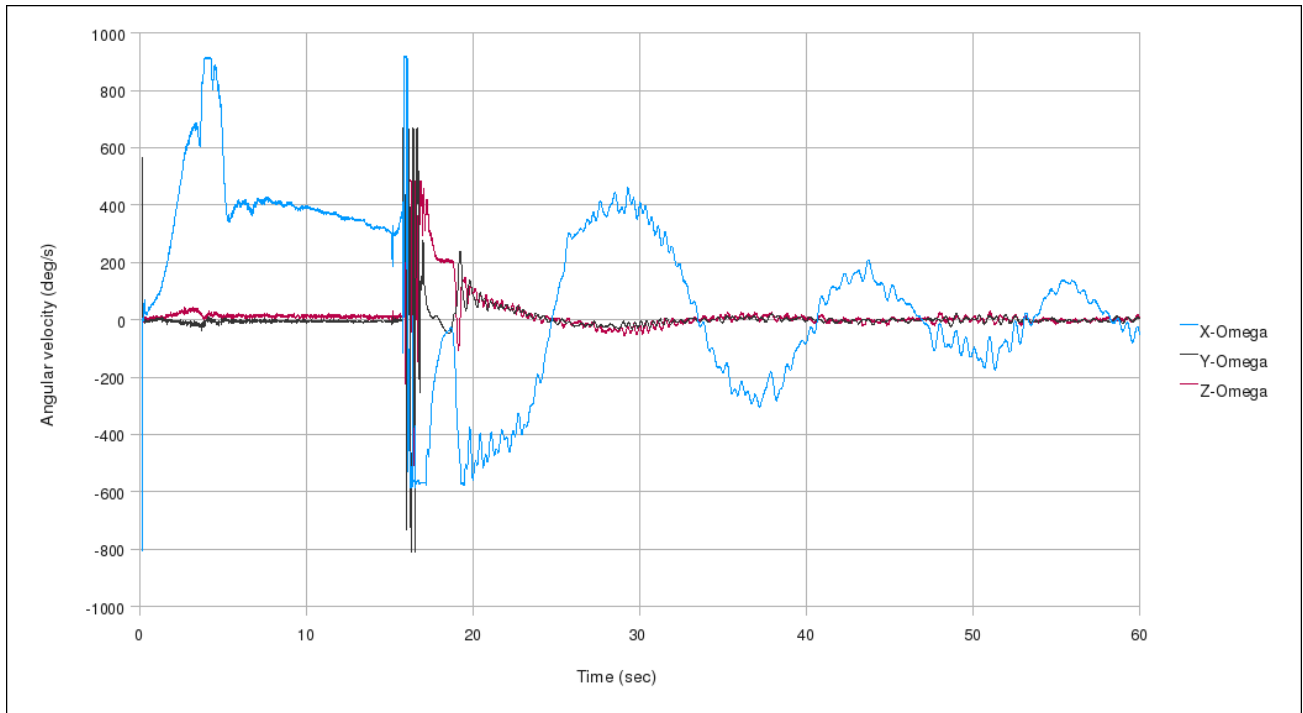


Figure 12 – Plot of angular accelerations about 3 axes during 1st minute of flight.

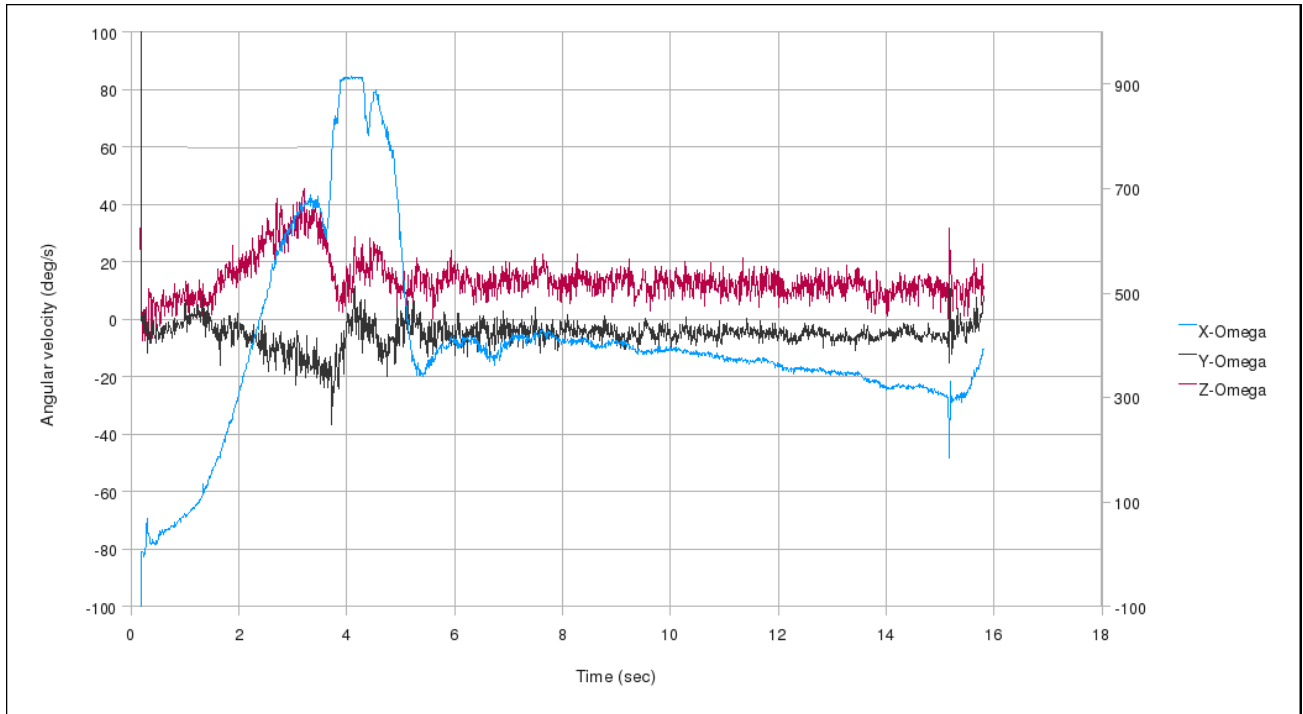


Figure 13 – Plot of angular accelerations plotted up to time of anomaly

The nosecone thermal data is plotted in Figure 14. Note that only inputs T0 to T4 were used (T5 was not connected). T1 did not successfully record thermal data. T0, T1, T2 and T3 sensors were mounted flush on the exterior of the nosecone skin. T4 was mounted inside the nosecone to measure internal temperature.

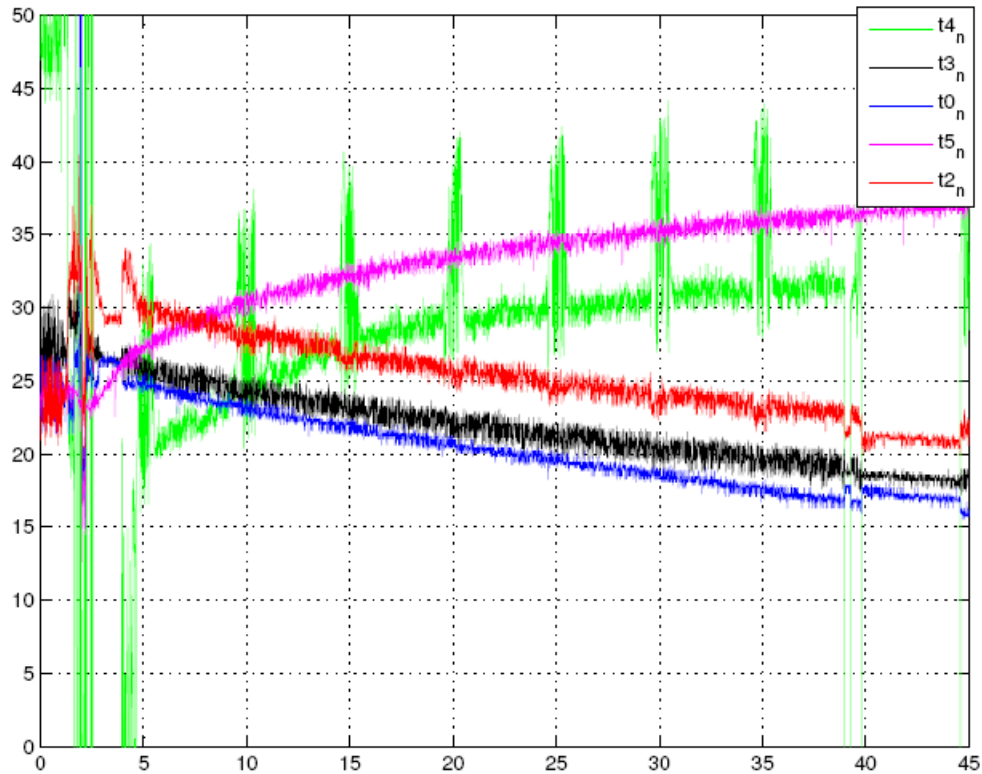


Figure 14 – Plot of nosecone thermal data

Analysis and Discussion of Flight Data

Liftoff time ($t = +0.000$) is taken from the Parrot data as the first time value with an acceleration value greater than the static value just prior to launch. This corresponds to an “offset” time value of 0.285 seconds for the Parrot data.

A common time base between the Parrot and the MC and CC is determined by matching the MC accelerometer data during the 2nd phase firing, and by matching the CC igniter events. The two key igniter events are

- 1) 2nd phase igniter activation
- 2) Loss of continuity of 2nd phase igniter and drogue igniter, which occur simultaneously

The flight event summary is shown below:

| <u>Event</u> | <u>Time (sec)</u> | <u>Ref.</u> | <u>Altitude AGL ft (metres) *</u> |
|--------------------------------|-------------------|----------------|-----------------------------------|
| Ignition | +0.000 | Parrot | 0 |
| Liftoff | 0.085 | Parrot | 0 |
| 1 st phase burnout | 4.05 | Parrot | 1414 (431) |
| 2 nd phase ignition | 15.16 | CC | 10240 (3121) |
| Motor rupture | 15.82 | MC | 10585 (3226) |
| Separation of Payload capsule | 16.16 | MC | 11697 (3565) |
| Main chute deployment | 16.26 | CC | 12209 (3721) |
| 2 nd phase burnout | ~25 | Ground video | unknown |
| Booster (fwd) ground impact | ~151 | On-board video | 0 |
| Main Chute pyro activate | 384.36 | CC | 240 (73) |
| Payload Capsule touchdown | 394.86 | CC | 0 |

* based on CC data

Table 5 – Flight events summary

From Figure 2, the Payload Capsule average descent rate was determined to be 29.4 fps (8.97 m/s) and touchdown velocity was 27.4 fps (8.36 m/s). This compares favourably with the design touchdown velocity of 32.2 fps (9.81 m/s).

It is apparent from Figures 9 to 11 that the vehicle was aerodynamically stable during the boost and coast phase right up to 2nd phase ignition.

Figure 15 shows the CC and Parrot altitude curves prior to and following the anomaly, as well as the key events of 2nd phase ignition, motor rupture and separation of the Payload Capsule from the Booster (as reported by the CC). Excellent agreement in apogee is seen between the CC and Parrot. Maximum CC altitude is 12,208 feet (3721 metres) AGL.

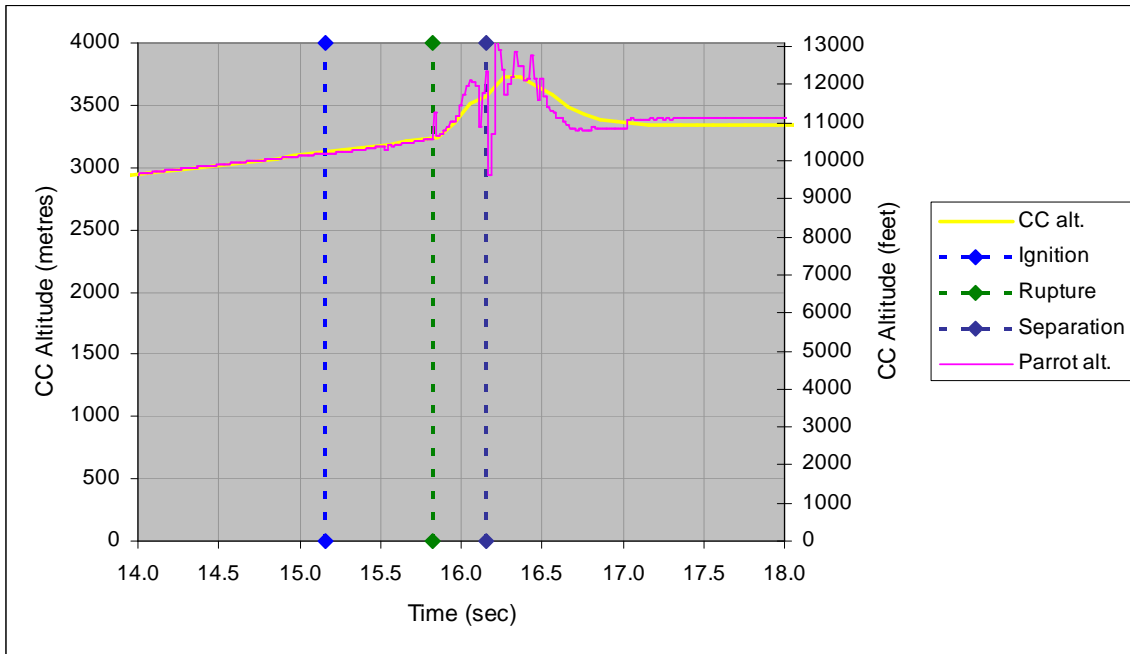


Figure 15 – CC and Parrot altitude prior to and following the anomaly, and key events of 2nd phase ignition

In Figure 16, the 1st phase thrust curve is derived from Parrot acceleration data and AeroLab drag data as used in the SOAR trajectory analysis. The simulation curve is obtained from SRM.XLS with the burn rate values adjusted to account for the specifics of the propellant as used for this flight. In particular, the “burn rate coefficient” was reduced due to the oxidizer being non-ground and non-desiccated. The simulated pressure curve is included to indicate the expected normal operating pressure of the motor design.

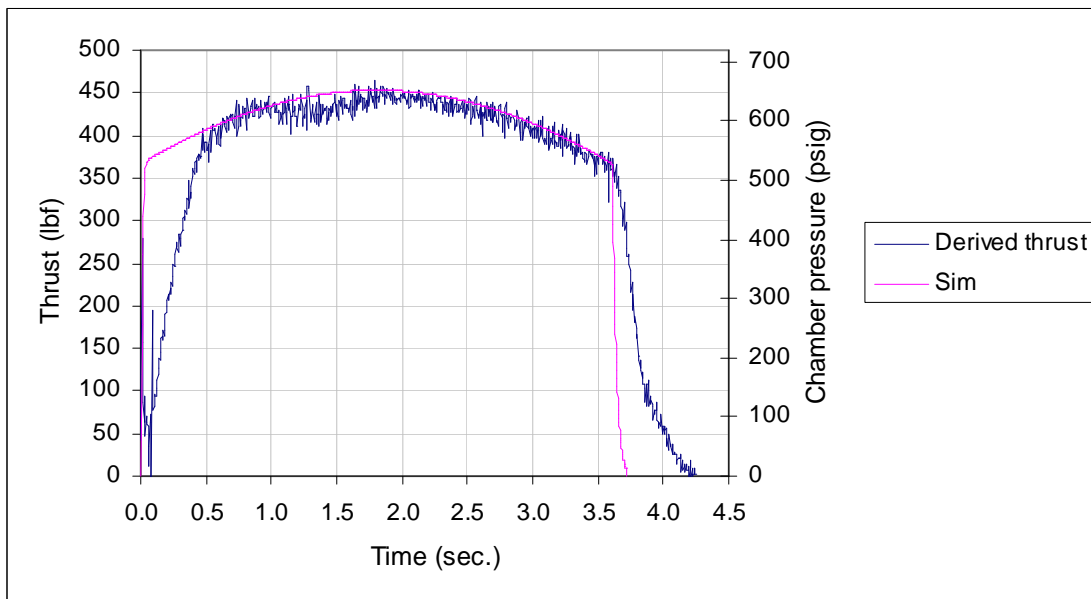


Figure 16 – Plot of derived motor thrust curve and simulation curve

Video footage – Ground-based video coverage of the entire ascent phase of the flight was taken by two participants. The excellent footage indicated that the vehicle was very stable during the climb toward second burn. This is in agreement with the low pitching accelerations shown in Figures 9, 10 & 11. Based on the disjointed smoke trail, the vehicle appears to have traversed a couple of layers of wind shear, particularly at the 4 second mark of the flight, which is also in agreement with the pitching acceleration per Figure 9. Shortly after 2nd phase ignition, a large cloud of smoke became visible, which can be attributed to the motor rupture. The odd looping motion of the rocket seen after that could have been a result of the Booster chute having been deployed nearly immediately after motor rupture, when the Payload Capsule was torn away from the Booster (see Table 5). The Booster chute, which was recovered in a shredded state, would have produced an offset drag and subsequent looping motion. The video shows that the looping suddenly stopped and the Booster section followed a more or less stable trajectory. This was likely the result of the Booster chute tether snapping and separating, allowing for stable flight for the remainder of the 2nd burn.

Excellent on-board video footage was also obtained. Although recording stopped abruptly when the forward Booster section impacted the ground, resulting in a file error, the file was successfully repaired. The footage, which showed an aft-facing view, showed the ascent to be nominal from liftoff until shortly after 2nd phase ignition. Smoke emanating from the Booster was visible during motor burn. The footage indicated a very stable climb, with an appreciable rate of roll which slowed after about 6 seconds. The roll rate was approximately constant at 1 rps until the anomaly occurred. From video analysis, the roll rates shown in Table 6 were obtained. The results are plotted in Figure 17 and are in good agreement with the angular acceleration indicated by the MC accelerometer, as seen in Figure 18.

| Rotations | comment | video frames | time (sec) | roll rate (rps) |
|-----------|-----------------|---------------------|-----------------------|------------------------|
| 1 | tower cleared | 50 | 1.67 | 0.6 |
| 2 | vertical ascent | 19 | 0.63 | 1.6 |
| 3 | vertical ascent | 14 | 0.47 | 2.1 |
| 4 | vertical ascent | 14 | 0.47 | 2.1 |
| 5 | vertical ascent | 10 | 0.33 | 3.0 |
| 6 | vertical ascent | 12 | 0.40 | 2.5 |
| 7 | vertical ascent | 15 | 0.50 | 2.0 |
| 8 | vertical ascent | 26 | 0.87 | 1.2 |
| 9 | vertical ascent | 24 | 0.80 | 1.3 |
| 10 | vertical ascent | 24 | 0.80 | 1.3 |
| 11 | vertical ascent | 24 | 0.80 | 1.3 |
| 12 | vertical ascent | 25 | 0.83 | 1.2 |
| 13 | vertical ascent | 26 | 0.87 | 1.2 |
| 14 | vertical ascent | 26 | 0.87 | 1.2 |
| 15 | vertical ascent | 27 | 0.90 | 1.1 |
| 16 | vertical ascent | 29 | 0.97 | 1.0 |
| 17 | vertical ascent | 29 | 0.97 | 1.0 |
| 18 | vertical ascent | 33 | 1.10 | 0.9 |
| 19 | motor rupture | 31 | 1.03 | 1.0 |
| | | 458 total | 15.27 total | 1.44 average |

Table 6 – Vehicle roll rate analysis from video footage

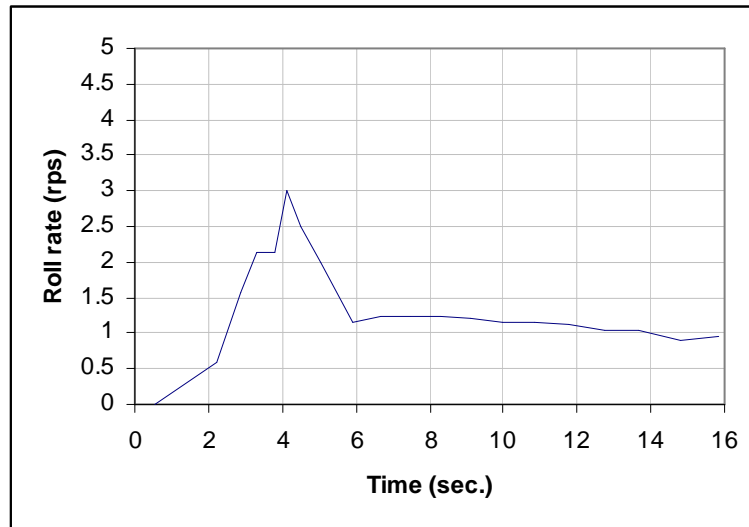


Figure 17 – Plot of vehicle roll rate data from video

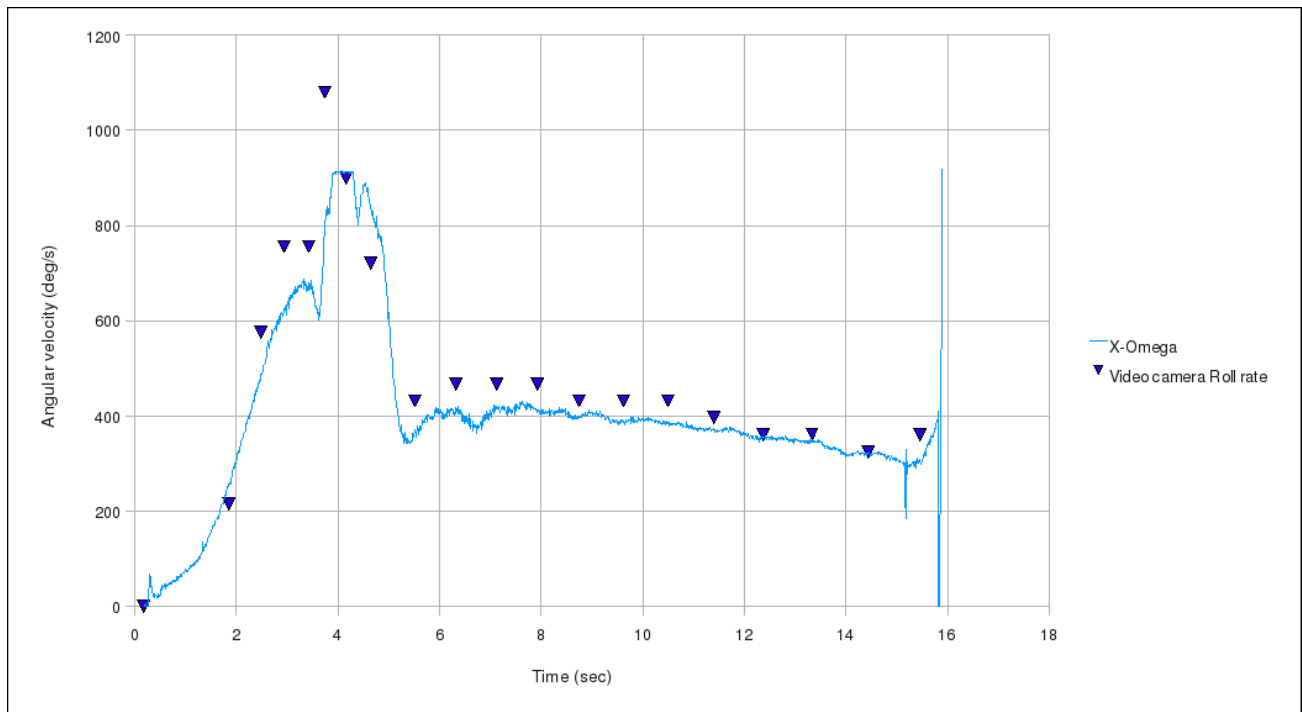


Figure 18 – Comparison of roll rate from MC and video

Burn of the 2nd phase was visually apparent by smoke emanating from the nozzle. The volume of smoke clearly increased throughout the brief burn, terminating with a large smoke cloud that accompanied the motor rupture. In the video footage, two spent casting tubes are seen being hurled (Photo x). The camcorder operation was not detrimentally affected by the violence of the event. During the descent, the footage captured the smoke emanating from the Mid-bulkhead, which served as a low-efficiency nozzle. The Booster section descended in a flat spin following burnout, and footage continued until impact with the ground. The impact velocity was estimated to be 111 ft/sec. (34 m/s) based on the fall time, from apogee to ground, of 95 seconds.

Thermal Data

The sensors mounted flush on the exterior of the nosecone skin all recorded a decay in temperature through the early portion of the flight. This is likely due to the lower ambient temperature at altitude. No thermal heating would be expected considering the nature of the flight.

The internal sensor showed a corresponding increase in temperature. This was likely due to the heat generated by the avionics. The “pulses” visible in the T4 data is likely due to beacon transmitter interference. The T4 leads were not shielded. The T0-T3 leads for the nosecone skin antenna were each shielded with aluminum tape, which apparently worked well.

Investigation of Primary Anomalous Event

The primary anomalous event was the rupture of the motor case during 2nd burn. The rupture was a result of structural failure of the aft motor casing/airframe at approximately mid-span due to pressure overload. Extrapolation of the pressure curve shown in Figure 8, which was clipped due to pressure sensor capacity being 1000 psig, suggests a rupture pressure of 1400 psig or greater. As a qualification for flight, both motor casings had been hydrostatically pressure tested to 1050 psig (72 bar). The ultimate design strength of the motor is 1800 psig (124 bar). The wound-fiberglass tubing (*Ameron Dualoy 3000/L*) from which the motor cases were fabricated, is structurally optimized to have equal strength in hoop and axial directions. The actual failure mode appeared to be axial. There is no evidence of significant flight loading (bending moment) superimposed upon the pressure loading leading to failure at lower than design rupture pressure. This is apparent from Figures 9 and 11 which show the pitching accelerations during the flight. The accelerations just prior to motor rupture are of a significantly lower magnitude than those during the initial portion of the flight (first 8 seconds or so), and as such, there is no indication of pitching which could have severely loaded the airframe in bending at that instant.

Figure 13, which illustrates the derived motor thrust curve in comparison to the simulation thrust & pressure curves, indicates that, overall, the 1st burn was of nominal performance. The performance was very similar to the *ProtoSShot III* static firing of July 25, 2009. The maximum chamber pressure was about 600 psig, based on the sim (actual chamber pressure was not measured). This is well below the maximum pressure achieved during the 2nd burn, which was >1400 psig. This provides evidence that the 2nd burn was severely anomalous, developing a chamber pressure well beyond the design condition.

In Figure 19, a plot of chamber pressure versus time is shown for the 2nd burn. Superimposed is the corresponding plot of chamber pressure that is taken from the *ProtoSShot III* static firing (Ref.5). It is seen that both curves initially climb at a comparable rate. At the 15.61 second mark, a sudden change in slope is seen to occur in the flight curve. After that, the slope remains essentially constant until sensor saturation just prior to rupture.

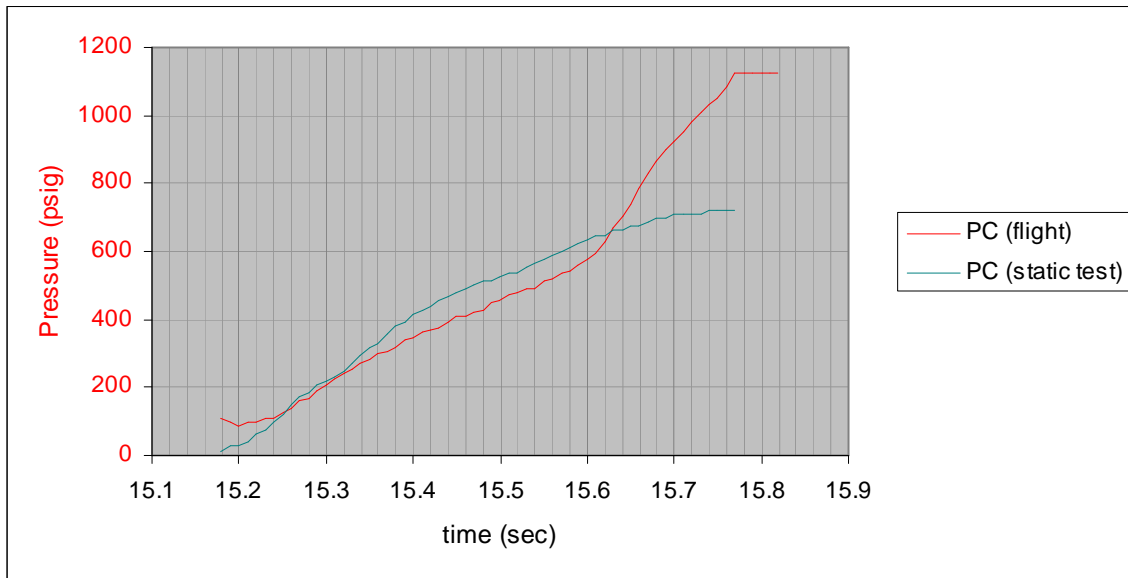


Figure 19 – Comparison between 2nd burn chamber pressure curves, flight versus static test

In order to understand what may have caused the sudden rise in chamber pressure, it is helpful to review the basic equation for chamber pressure for a solid rocket motor.

Chamber pressure, P_c , developed in a rocket motor is given by the equation below:

$$P_c = K_n \rho r c^* \quad \text{equation 1}$$

Where K_n is the ratio of propellant burning area to throat cross-sectional area ($K_n = A_b/A_t$), ρ is the propellant density, r is the burn rate and c^* is characteristic exhaust velocity of the propellant.

Based upon the now-standardized propellant used in the motor, and the fact that the 1st burn was nominal, it can be safely assumed that sudden change in burn rate was not the cause of the deviant chamber pressure rise seen in the 2nd burn. Nor would propellant density or characteristic velocity, as both of these parameters are constants for a given propellant.

This leaves either the throat cross-section area as being reduced, for example through partial blockage, or an increase in burning area, for example through cracked or disbonded propellant.

The nozzle blockage scenario is considered first. If the throat is restricted and the cross-sectional area effectively reduced, this would reduce the thrust output of the motor, since there is a direct relationship between the two as follows.

$$F = C_f A_t P_c \quad \text{equation 2}$$

Where F is thrust, C_f is thrust coefficient and A_t is the throat cross-sectional area. Note that the thrust coefficient can be considered to be a constant. If the thrust is reduced due to a restriction in throat area, acceleration of the vehicle would be directly reduced as a consequence.

Figure 20 shows a plot of vehicle acceleration versus chamber pressure during and immediately after the motor rupture. Notice that the chamber pressure readings are invalid after the 16.1 second mark,

when the sensor leads were severed due to separation of the Payload Capsule from the Booster. During the burn, as chamber pressure rises, vehicle acceleration rises correspondingly. This response is illustrated more clearly in Figure 21, where the graph y-scales are selected appropriately to compare slopes of the two curves. The slope of the acceleration curve leading up to, and following, the sudden change in pressure rise, is seen to match the slope of the pressure curve, indicating that thrust is maintained as expected for a nominal (non-restricted) throat size.

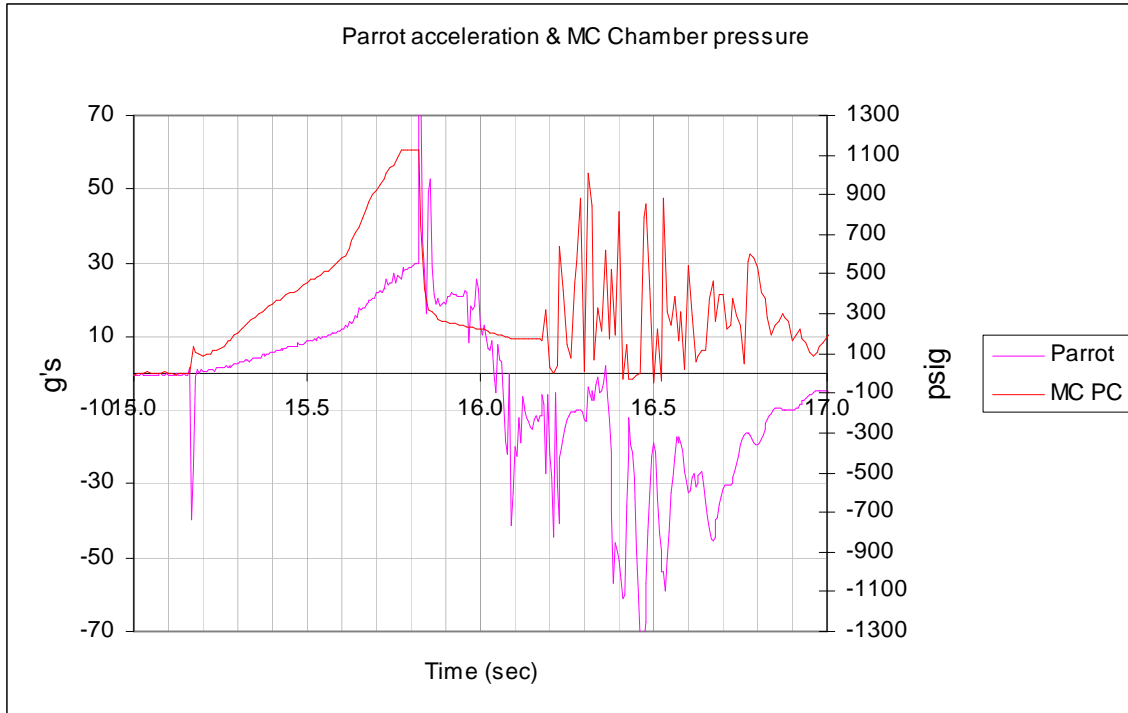


Figure 20 – Vehicle acceleration versus chamber pressure

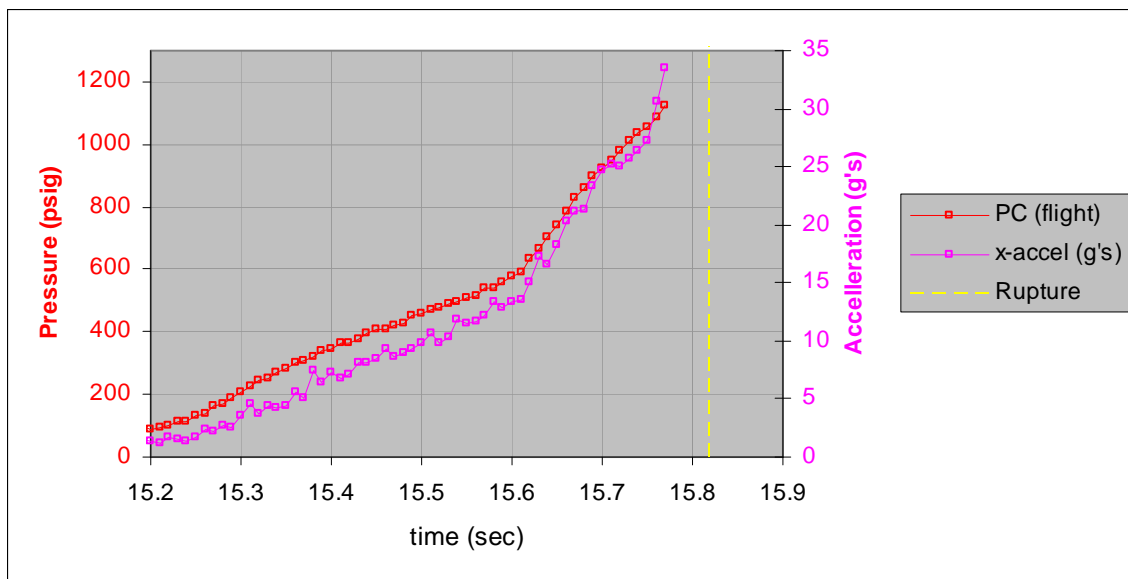


Figure 21 – Vehicle acceleration as compared to chamber pressure during 2nd burn.

As further evidence of the throat being non-restricted, Figure 22 shows that the vehicle acceleration, based on calculated performance, assuming a nominal throat size, matches quite well the measured

acceleration. The calculation was based on equation 2 (using $C_f=1.6$ from static test) and utilizing the equation of motion

$$F = \text{mass} \times \text{acceleration} \quad \text{equation 3}$$

And where mass was adjusted to vary due to propellant consumption. Figure 23 illustrates the effect upon vehicle acceleration for varying degrees of assumed nozzle blockage, assuming blockage is present from the moment the 2nd burn begins.

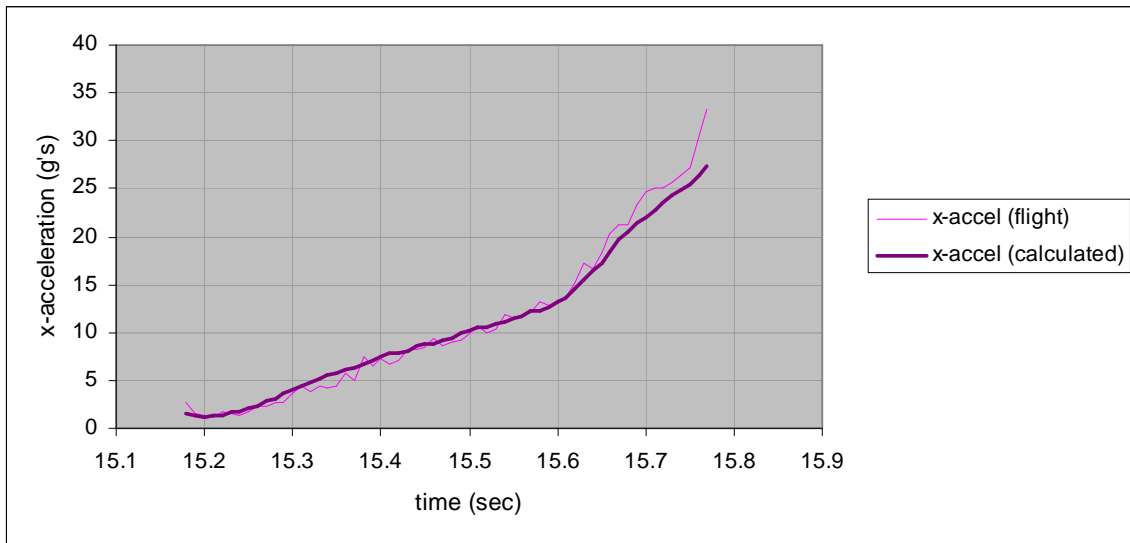


Figure 22 – Actual versus calculated acceleration based on nominal throat size.

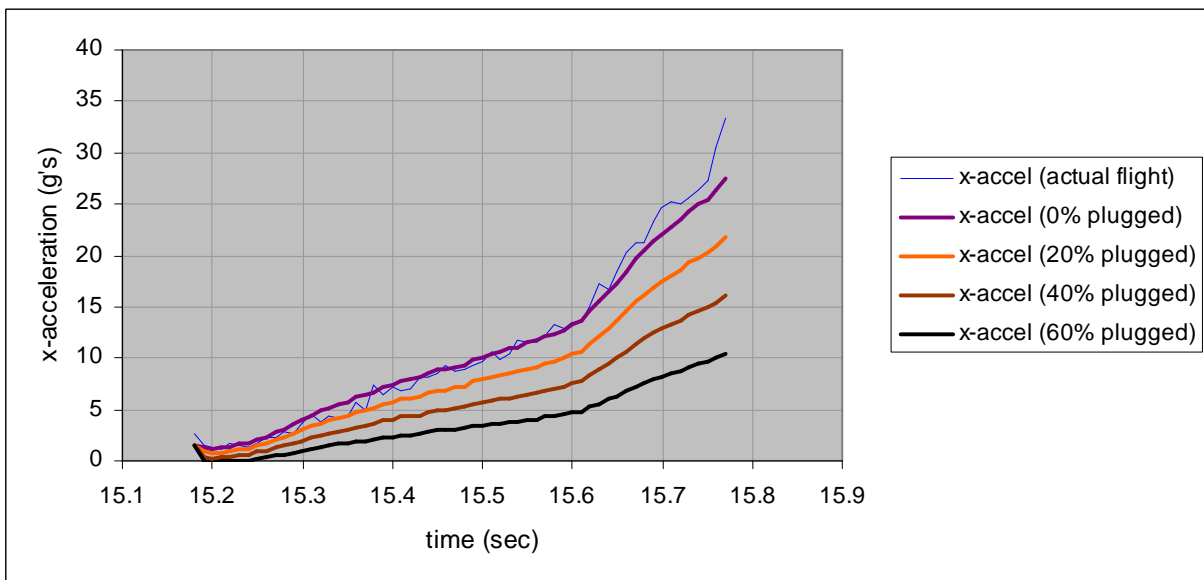


Figure 23 – Actual versus calculated acceleration based on various degrees of throat blockage

In Figure 24, the same analysis is presented, however, hypothetical blockage is assumed to suddenly occur at the 15.6 second mark, where the sharp change in slope begins. It is seen in the plot that a

distinct drop in acceleration would accompany such a hypothetical condition, which is contrary to the actual flight data. Based on this analysis, there is no evidence of nozzle blockage at any point during the 2nd burn. As final evidence, a frame-by-frame analysis of the on-board video footage clearly shows an ever-increasing amount of smoke emanating from the nozzle right up to the instant of rupture.

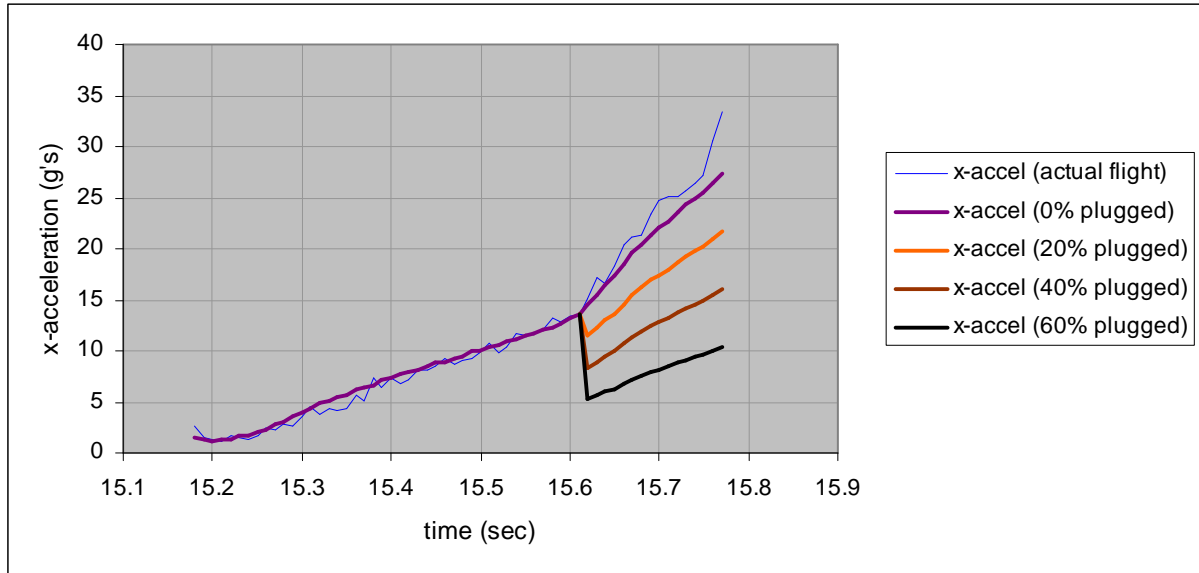


Figure 24 – Actual versus calculated acceleration based on restricted nozzle throat.

The second scenario, whereby the propellant burning area begins to increase at the 15.6 second mark, is examined next. The two most obvious means by which this can occur would be a crack (or numerous cracks) or by propellant disbonding or separation at the propellant/casting tube interface (the ablative casting tubes also serve as burn inhibitors).

Cracks or disbonds being initially present (prior to launch) is considered unlikely due to high standard of propellant manufacturing, similar or better to that used in the static firings. Additionally, quality control inspections were conducted which visually inspected for signs of cracks and for inhibitor disbonding (coin tap test). The high propellant density that was obtained precluded any significant bubbles, voids or porosity. And considering that the 1st burn was nominal, the only reasonable scenario would be to consider cracks or disbonding to have occurred in flight.

It is apparent that disbonding of the propellant from a casting tube exposes more surface area than a single crack through the propellant web. In such a case, assuming complete disbonding, the entire outside surface of a grain would be exposed. As such, this is the scenario that is examined in the following analysis.

Rocket motor design software SRM.XLS was modified to simulate any number of fully-disbonded grain segments. The assumption used was that the entire outer surface of a grain segment would be exposed and immediately started burning. This would be the scenario if the casting tube had completely failed to inhibit burning and thus added more burning area. Figure 25 illustrates the outcome of this analysis, for 0, 1, 2 or 3 failed grain segments.

As can be seen, a complete casting tube failure of 3 grain segments would be necessary to develop chamber pressure high enough to account for the anomalous pressure level seen in flight. A post-flight dissection and detailed examination of the recovered forward casting tubes indicated that none were cracked or broken and suffered only the expected amount of thermal degradation based on the extended burn duration of the 2nd phase.

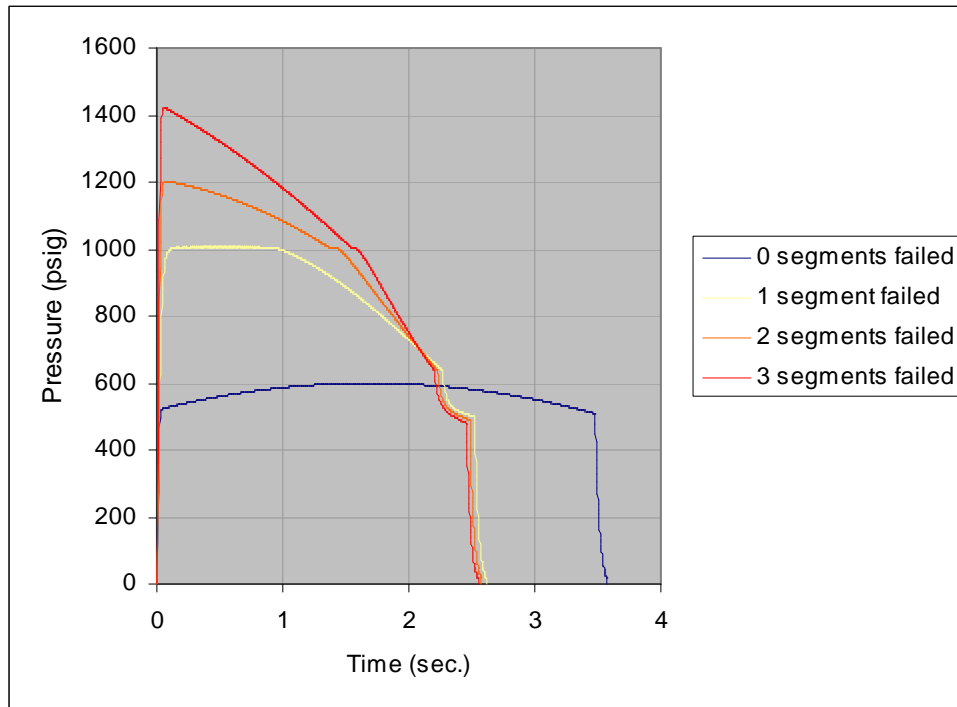


Figure 25 – Chamber pressure variation with fully-disbonded grain segments.

The likelihood that 3 of the 6 grain segments fully-disbonded would seem unlikely, unless there was a common cause. There is a hypothetical scenario whereby this could occur. If pressure equalization around the grain assembly did not happen rapidly enough, the resulting pressure differential between the interior and exterior of the grain assembly could conceivably be high enough to bulge the casting tubes outward, as illustrated in Figure 26 (shown exaggerated). Such a scenario could lead to multiple disbonding, if the bond between propellant and casting tube is weak. If the bond is strong, such a condition could instead lead to compound cracking of the propellant.

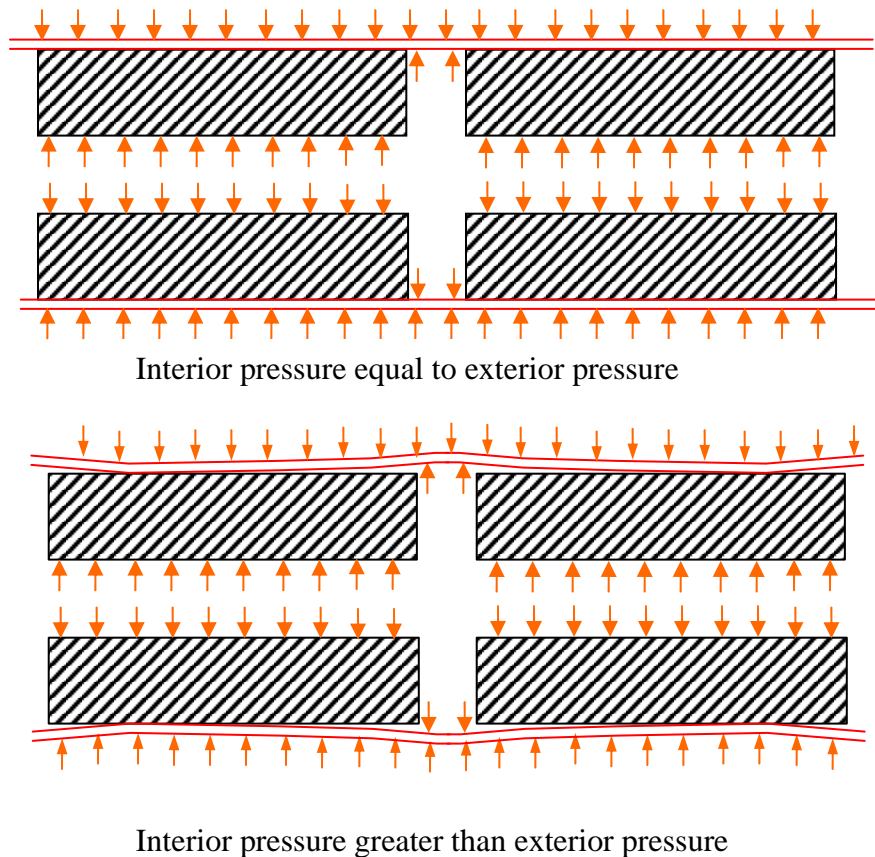


Figure 26 – Illustration of possible grain disbonding due to non-equalized pressure

Possible Secondary Anomalous events

An examination of the vehicle axial acceleration during the 1st phase burn, as shown in Figure 5, reveals a curious spike about a third way into the burn. The Parrot records this as a decrease in acceleration, yet the MC records this as a positive spike. The two spikes do not coincide exactly, separated by perhaps 50 milliseconds. As such, these may be two separate but related events.

It is also noticed that there is a distinct change in the trend of the acceleration curve following this event, increasing slightly then leveling off.

Since there was no provision for chamber pressure measurement during the 1st burn, it is unknown whether this was a motor initiated event (e.g. ejection of a fragment) or some other event that momentarily affected the vehicle flight dynamics.

Another apparent anomaly relates to the main parachute pyro being fired by the CC at an altitude of 73 metres. This is significantly lower than the altitude it was to be fired, which was 400 metres (with a default time of 750 seconds). However, a review of the CC performance indicated that this delayed triggering of the main parachute pyro was not anomalous, rather, was a result of the CC

software trajectory programming which catered to a nominal flight. The non-nominal nature of the flight led to this result.

Conclusions

Excellent flight data was recorded by the three on-board sensing/recording devices – *Featherweight Parrot*, Main Computer and Chute Controller. Good agreement between the devices was achieved. The GPS data suffered from intermittent and inaccurate data. This could be a result of interference with the beacon transmitter antenna which was in close proximity to the GPS antenna. Telemetry did not perform very well with minimal data received by the ground crew. A possible culprit is the patch antenna. As such, ground testing should be conducted and the problem rectified prior to next flight. The Chute Controller successfully fired the 2nd burn of the motor. The drogue and main chute triggering also worked, although the anomalous nature of the flight did not allow for a rigorous test of this functionality. The main parachute was deployed much later and closer to the ground than intended, due to the nature of the trajectory modeling. This should be revised before next flight to better cater to a non-nominal flight, if feasible.

The achieved altitude of the rocket compared well to the flight simulations.

The radio beacons were tracked fairly well. However, due to the anomalous nature of the flight, a conclusion cannot be drawn as to how well the tracking would have succeeded had the altitude goal been achieved. There were valuable lessons learned regarding tracking and recovery which can be utilized for the next *MiniSShot* launch event.

Excellent ground-based and on-board video footage of the flight was obtained, which was of great value in assessing the flight, aiding to validate the instrumentation data, and investigating cause of the primary anomaly.

The data suggests that the vehicle was fully stable throughout the flight right until the moment of breakup. Breakup was likely a result of aerodynamic forces which imposed undue bending loads on the forward airframe after motor rupture (following rupture, the forward airframe lacked fins to maintain a stable trajectory).

The first burn of the motor performed well and in a manner very similar to the earlier static firing. The motor experienced abnormally high chamber pressure shortly after 2nd phase ignition which exceeded the structural capacity of the aft motor casing. It is unknown why the motor casing ruptured at a pressure apparently below the ultimate structural capacity of the tube. Thermal heating may have played a role, although it would have seemed more likely, if that was the case, to have failed closer to the Mid-bulkhead where static testing clearly indicated the highest thermal loading occurs.

Based on the analyses presented, the flight data provides no evidence of partial or complete nozzle blockage to explain the over-pressurization.

Complete disbonding of at least 3 grain segments would be required to generate chamber pressure sufficient to match that experienced by the anomalous 2nd burn. Cracking of one or more grains would not provide enough burning area to account for the level of pressure seen unless compound

grain fracture occurred. Disbonding of the “topped off” portions of the propellant grains would likewise not generate enough surface area to account for the over-pressurization.

In addition to actual disbonding of propellant from a casting tube, a separation or crevice would be necessary for the flame front to propagate. Since there was no physical evidence of casting tube cracking or other fracture, the only possible means for separation to occur would be if the grain assembly was subjected to non-equalized pressure around its periphery. Due to the high elastic modulus of sugar propellant, it is not capable of deforming significantly (without fracture) if structurally overloaded. As such, the design of the motor relies upon a spacing, or gap, between the grain assembly and the chamber walls, which is required to rapidly fill up with combustion gases upon motor startup, to equalize the pressure inside and outside the grain assembly. If for some reason this pressure equalization did not occur or was delayed, the internal pressure in the grain assembly could tend to cause the casting tube assembly to expand outward, which would result in a likelihood of breaking the bond between propellant and casting tube. Such a scenario may result in sufficient burning area if this occurred to a minimum of 3 of the 6 grain segments and if the exposed propellant ignited immediately.

Dedicated testing of propellant grain and casting tube behaviour under structural loading is planned. This will hopefully shed light on the feasibility of the hypothesized causes of the anomaly. No firm conclusions can be drawn at this time.

References

1. MiniSShot Trajectory Study
http://sugarshot.org/downloads/minisshot_trajectory_study_20091115.pdf
2. MiniSShot Trajectory Study using SOAR
http://sugarshot.org/downloads/SS2S_MiniSShot_Trajectory_SOAR_study.pdf
3. MiniSShot Vehicle MassStatement: Iteration 2
http://sugarshot.org/minisshot_mass_statement_iteration_2.pdf
4. MiniSShot Rocket Vehicle Assembly, Launch Preparation & Procedure Manual
<http://sugarshot.org/downloads/MiniSShot%20Assembly%20Manual%202010-03-23.pdf>
5. ProtoSShot-M Mark III Rocket Motor
Report of Static Test Firing of July 25, 2009
http://sugarshot.org/ProtoSShot_III_firing_report.pdf
6. MiniSShot Rocket Motor Assembly and Propellant Loading Manual
http://sugarshot.org/downloads/MiniSShot_Motor_Assembly_Manual_2010-03-10.pdf
7. MiniSShot Pyrotechnic Separation Device Assembly Manual
http://sugarshot.org/downloads/MiniSShot_PSD_Assembly_Manual_2010-03-01.pdf
8. MiniSShot Avionics Block Diagram: Version 5
<http://sugarshot.org/MiniSShot%20Block%20Diagram%20V5.pdf>
9. MiniSShot Main Computer Manual
http://sugarshot.org/downloads/minisshot_main_computer_manual_20090419.pdf
10. MiniSShot Chute Controller manual
http://sugarshot.org/downloads/MiniSShot_chute_controller_manual_20091222.pdf
11. Big Red Bee “BeeLine” Configuration Checklist
http://www.sugarshot.org/downloads/beeline_checklist.pdf
12. Featherweight “Parrot” Configuration & Checklist
http://www.sugarshot.org/downloads/parrot_checklist_a.pdf
13. MiniSShot Telemetry Instructions
http://sugarshot.org/downloads/MiniSShot_Telemetry_instructions_rev.pdf
14. MiniSShot Chute Controller Instructions
http://sugarshot.org/downloads/MiniSShot_chute_controller_instructions_20100124.pdf
15. MiniSShot Main Computer Instructions
http://sugarshot.org/downloads/MiniSShot_main_computer_instructions_20100123.pdf

16. MiniSShot Wiring Harness Guide

http://sugarshot.org/downloads/MiniSShot_Wiring_Harness_Guide_2010-03-10.pdf

17. MiniSShot Video Camcorder Operation & Set-up Manual

http://sugarshot.org/downloads/MiniSShot_Camcorder_Manual_2010_03_10.pdf

18. April 25, 2010 Sugar Shot Tracking/Recovery Debrief

http://sugarshot.org/downloads/April_25_2010_SugarShot_Tracking_Recovery.pdf

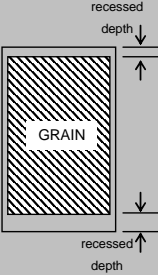
Appendix A

MINISSHOT GRAIN DENSITY CHECK

Casting tube inner diameter = mm
 Core diameter = mm

Grain ideal density = 1.841 g/cc

INSTRUCTIONS: FILL IN DATA IN WHITE CELLS



| Grain s/n | Mass of casting tube (grams) | Mass of casting tube + propellant (grams) | Length of casting tube (mm) | Recessed depth Top (mm) | Recessed depth Bottom (mm) | Grain length (mm) | Mass of propellant (grams) | Grain density ratio (actual/ideal) |
|-----------|------------------------------|---|-----------------------------|-------------------------|----------------------------|-------------------|----------------------------|------------------------------------|
| 1 | 121.7 | 1043 | 145.5 | 9.5 | 8.0 | 128.0 | 921.3 | 96.2% |
| 2 | 105.7 | 1016 | 145.5 | 12.5 | 8.0 | 125.0 | 910.3 | 97.3% |
| 3 | 109.2 | 1011 | 145.5 | 11.0 | 9.0 | 125.5 | 901.8 | 96.0% |
| 4 | 109.7 | 1004 | 145.5 | 11.5 | 10.0 | 124 | 894.3 | 96.3% |
| 5 | 111.5 | 1026 | 145.5 | 11.0 | 8.5 | 126 | 914.5 | 97.0% |
| | | | | | | | | |
| 1 | 109.2 | 1026 | 144.5 | 10.5 | 8.0 | 126 | 916.8 | 97.2% |
| 2 | 80.0 | 997 | 144.0 | 11.0 | 8.0 | 125 | 917.0 | 98.0% |
| 3 | 80.8 | 1001 | 144.0 | 11.0 | 8.0 | 125 | 920.2 | 98.3% |
| 4 | 104.3 | 1000 | 143.0 | 10.0 | 11.0 | 122 | 895.7 | 98.1% |
| 5 | 80.9 | 1000 | 143.0 | 9.0 | 9.0 | 125 | 919.1 | 98.2% |
| 6 | 97.5 | 979 | 143.7 | 13.5 | 9.5 | 120.7 | 881.5 | 97.6% |
| 7 | | | | | | 0 | 0.0 | |
| 8 | 108.5 | 1017 | 144.5 | 8.5 | 9.5 | 126.5 | 908.5 | 95.9% |

Yellow highlighted cells represent grain segments used for the aft chamber.

Acknowledgements of Launch Event participants

MiniSShot launch team:

Paul Avery
Matt Campbell
Chris King
Rick Maschek

Other Sugar Shot personnel:

Grant Saviers

SAR participants & compatriots:

David Hedd
Mark Kern
Mark Kinsey
Jeff Lehman
John Metzger
John Norman
Travis Puderbaugh

Stratofox:

Ian Kluft
TBA

Non-affiliated:

Ken Mannat
Ken Brown
Barbara Bailey

FAR:

Dok Hansen
John Newman
Ted Rothaupt

Photographs/video:

Rick Maschek
Barbara Bailey
Jerry Irvine
Travis Kallahar

Photos



Photo 1 – Propellant grain segments

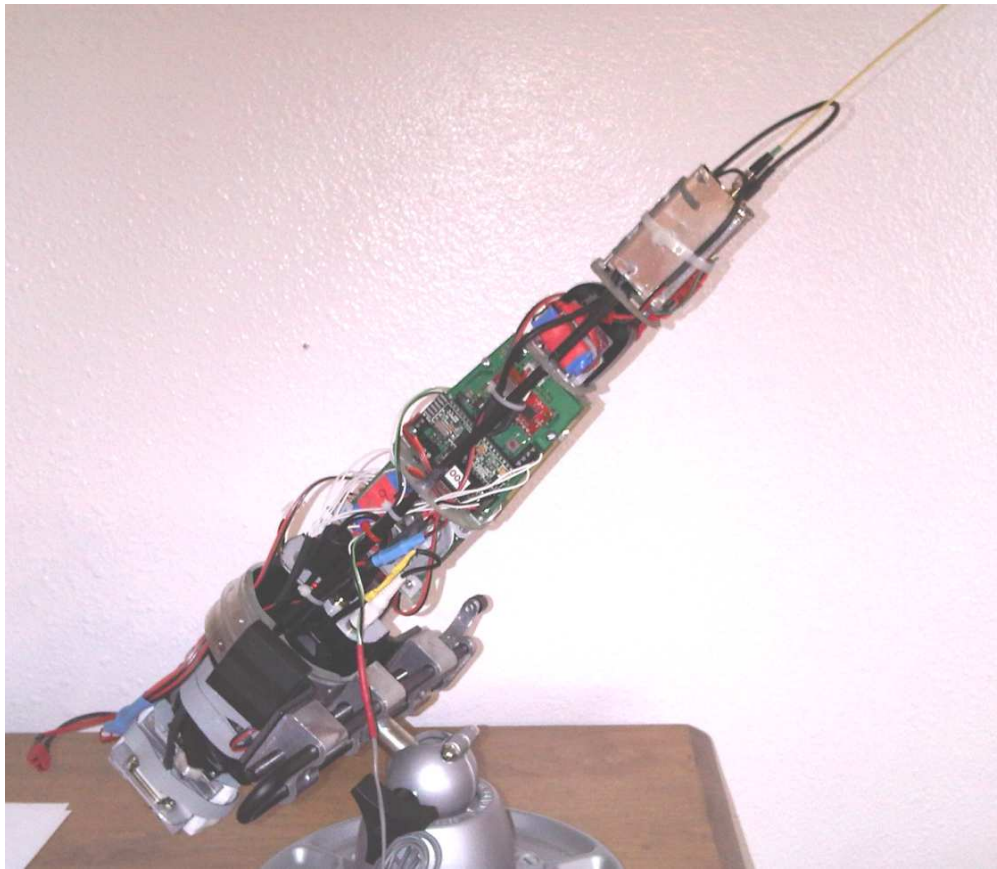


Photo 2 – Avionics assembly



Photo 3- FAR test site in the Mojave Desert, California



Photo 4 – Rick Maschek assembling motor



Photo 5 – Rick Maschek with the assembled Booster motor



Photo 6 –Forward Avionics ready to be installed in rocket



Photo 7 – Rick Maschek and Chris King preparing to install Forward Avionics in rocket



Photo 8 – Assembling the Aft Avionics

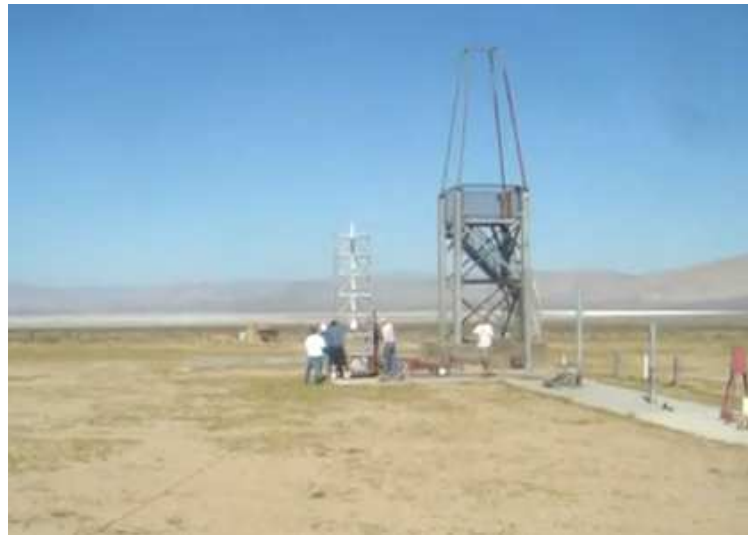


Photo 9 – Raising the launch tower to vertical firing position.



Photo 10 – Rocket in the launch tower just prior to liftoff



Photo 11 – Liftoff of MiniSShot at 10:03 PDT



Photo 12 – Soaring skyward straight & true



Photo 13 – Shortly after anomaly, vehicle loops twice, then trajectory straightens out



Photo 14 – Payload Capsule about to safely touch down



Photo 15 – Payload Capsule safely on ground



Photo 16 – Chris King at landing site of Booster aft section



Photo 17 – Recovered sections of Booster



Photo 18 – Aft (finned) section of Booster



Photo 19 – Back at the FAR site, Paul Avery examines Booster



Photo 20 – Search and Recovery team



Photo 21 – Still captures from on-board video footage

Top left: Vehicle in the launch tower prior to liftoff

Top right: Vehicle accelerates away from launch complex

Middle left: Following burnout, vehicle coasts

Middle right: Second phase firing

Bottom left: Following motor rupture, finned portion of Booster & 2 casting tubes seen falling away

Bottom right: Second burn continues with smoke exiting through Mid-bulkhead



Photo 22 – Still captures from on-board video footage (continued)

Top left: View of ground terrain during Booster descent, shortly after apogee

Top right: View of initial smoke trail from 2nd burn

Bottom left: View of ground terrain during Booster during plummet to ground

Bottom right: One of the last frames taken just before impact



Photo 23 – Forward casting tubes after cleaning and splitting open for examination

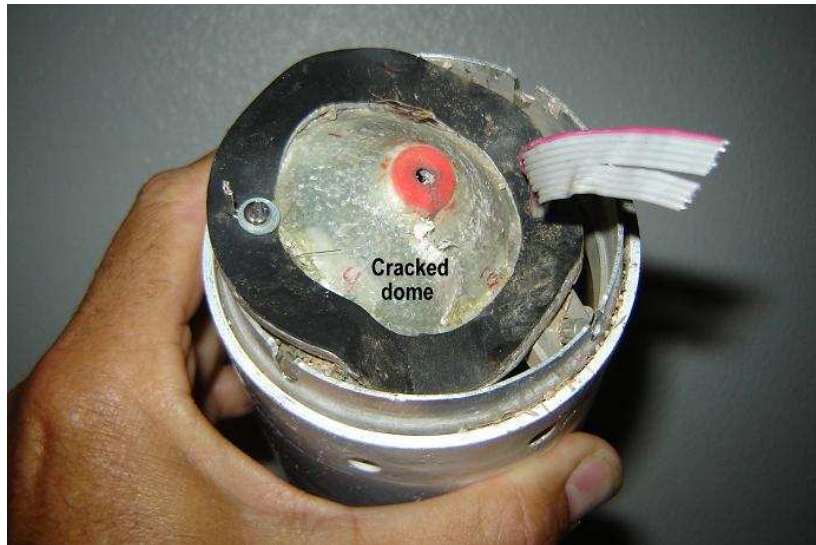


Photo 24 – PSD dome damage due to ground impact



Photo 25 – PSD damage



Photo 26 – Coupler shear tear-out damage at PSD retention pins